공학석사학위논문

서수 패턴분석을 통한 스트레인 웨이브 기어 기반 로봇 팔 접합부 진단 프레임워크

A Diagnosis Framework for the Robotic Arm Joint with Strain Wave Gearing based on Ordinal Pattern Analysis

2021 년 8 월

서울대학교 대학원

기계공학부

이 동 규

서수 패턴분석을 통한 스트레인 웨이브 기어 기반 로봇 팔 접합부 진단 프레임워크

A Diagnosis Framework for the Robotic Arm Joint with Strain Wave Gearing based on Ordinal Pattern Analysis

지도교수 윤 병 동

이 논문을 공학석사 학위논문으로 제출함

2021 년 4 월

서울대학교 대학원

기계공학부

이 동 규

이 동 규의 공학석사 학위논문을 인준함

2021 년 6 월

위 원 장 : 김 윤 영

부위원장 : 윤 병 동

위 원 : 김 도 년

Abstract

A Diagnosis Framework for the Robotic Arm Joint with Strain Wave Gearing based on Ordinal Pattern Analysis

Dongkyu Lee
Department of Mechanical Engineering
The Graduate School
Seoul National University

With the fourth industrial revolution, a smart manufacturing system has been adopted in many enterprises and the demand for health assessment of industrial robots has skyrocketed in various industrial sectors. In this context, the conventional study has focused on diagnosing robots based on the physical dynamic model and vibration signal. However, 1) the approximate model had intrinsic modeling uncertainty, 2) the vibration signal could be disturbed by external noise, and 3) the motion preprocessing and physical reasoning of health assessment have not been well organized. In addition, Strain wave gear (SWG) has not been considered of health assessment although it has been used for many years as a speed reducer due to its high performance. Its elastic flexspline has been susceptible to fatigue failure causing gear backlash.

In this study, therefore, we measure the motor input current of a robotic arm joint to make it less susceptible to external noise. Also, we propose a diagnosis framework of robots with SWG gearing based on ordinal pattern analysis with optimal parameter selection considering physical interpretation. The framework is composed

of the following steps: 1) Motion Segmentation based on Time-Frequency Representation (TFR), 2) Ordinal Pattern Analysis of Motor Current (OPAMC), and 3) Distribution-based fault detection.

At first, in the motion segmentation process, the motor current signal is frequency-demodulated using Temporal Fine Structure (TFS) since the robot's joint speed has a linear relationship with the current signal's frequency component. Also, the TFS is analyzed in the time-frequency domain to formulate a normalized motion signal which is used to decompose the current signal into multiple segments. Then, the segments are identified into different types of motions based on the similarity with reference motions. Also, the total number of cycles and motion types are calculated in this process. Secondly, in OPAMC, the segments are time-synchronized with reference motion and Hilbert-transformed to get an envelope for ordinal pattern extraction. Using a fundamental frequency of the current signal, the optimal parameter is calculated, and the ordinal patterns are extracted in the form of probability mass function (PMF). Then, the PMF of an observed state is quantitatively compared with a normal state through Jensen-Shannon divergence (JSD). Finally, each JSD distribution among different joints is represented on 3-dimensional feature space through point estimate of mean and variance and Kolmogorov-Smirnov statistics whose dimension is then reduced to 1 dimension scalar through linear discriminant analysis.

For validation, it is tested on two cases of control condition, increasing velocity 20, 50, 100% and payload 0,1,2 kg. Also, the optimal parameter for extracting ordinal patterns is compared with actual values to demonstrate its feasibility. On velocity control, the JSD shows to be higher on the faulty reducer, and its distribution shows a distinct difference between normal and faulty joint on all speed conditions. However, on the payload control condition, the JSD is only higher with no payload mounted than the payload on the fault SWG. The payload caused less modulation on

torque and motor current, and thus fewer backlash characteristics appeared on ordinal patterns.

In this research, a diagnosis framework is proposed with the motion segmentation and optimal parameter in ordinal pattern extraction. Since it is subjective to diagnose the robot with a simple threshold, the comparative analysis among different joints shows to be more efficient in terms of rational health assessment. Also, the framework is validated on various operating conditions such as velocity and payload condition yielding high reliability on the study.

Keyword: Industrial robot
Strain wave gear
Diagnosis framework
Ordinal pattern analysis
Motion segmentation
Distribution-based fault detection

Student Number: 2019-22571

Table of Contents

List of Tables

List of Figures

Nomenclatures

CWT	Continuous Wavelet Transform
FT	Fourier Transform
STFT	Short Time Fourier Transform
TFR	Tme-Frequency Representation
TFS	Temporal Fine Structure
CTFS	CWT of Temporal Fine Structure
OPAMC	Ordinal Pattern Analysis of Motor Current
JSD	Jensen-Shannon Divergence
KLD	Kullback-Leibler Divergence
LDA	Linear Discriminant Analysis
SWG	Strain Wave Gear
HT	Hilbert Transform
MCSA	Motor Current Signature Analysis
KS	Kolmogorov-Smirnov
D_n	Divergence from n-length reference
F_n	Function of n-length data
F_{obs}	Function of observed data

PDF	Probability Distribution Function
CDF	Cumulative Distribution Function
S_b	Between-class scatter matrix
S_w	Within-class scatter matrix
S_t	Total-class scatter matrix
m_k	Class mean of *k*-th class
m	Global mean of all class
$\vec{V}_r$	Variance vector of reference segment
$\vec{V}_t$	Variance vector of target segment
sim^k	Cosine similarity of *k*-th step
x_r	Segmented signal in reference motion
x_t	Segmented signal in target motion
f_s	Sampling frequency
f_d	Fundamental frequency
τ	Time delay parameter
τ_{opt}	Optimal time delay parameter
α	Order of ordinal pattern
$\pi_\alpha^\tau(t)$	Ordinal pattern with α and τ at time t

Chapter 1. Introduction

1.1. Motivation

Since the industry 4.0 accelerated the spread of smart factories, the industrial robots have been adopted in various industrial sectors. The automated production line transformed to be more complicated and dependent each other, and downtime could cause enormous economic loss to the company. Therefore, diagnosis and health management of manufacturing system such as industrial robot has become a major issue [1].

A conventional method for diagnosing robot's health condition has been model-based approach where robot's behavior approximate into dynamic model. However, such method had intrinsic modelling uncertainty that the model could not fully describe the actual behavior of robot's motion [2]. Another approach has utilized the vibration signal measured on gearbox of RV speed reducer, but it had disadvantages that only constant speed condition was considered, and non-stationary signal was difficult to diagnose. Also, the external noise could hinder health assessment of robot joint [3]. The other approach to deal with noise issue was measuring motor current on robot joint with RV reducer and analyzing with wavelet decomposition method [4]. Envelope and Time-Frequency Representation (TFR) of motor current was also implemented to diagnose the robot's health status in an unsupervised manner [5]. The motor current was less susceptible to external noise rather than vibration signal and could represent the robot's health condition under non-stationary condition.

However, these approaches could hardly render physical meaning in parameter selection and lacked in establishment of preprocessing method such as motion segmentation. Also, the Strain Wave Gear (SWG), one of the commonly used speed reducers in industry, has not been considered in previous studies.

1.2. Scope of research

This research takes advantage of noise robustness in motor current and suggests diagnosis framework of robotic arm joint with SWG. In first step, the motor current is frequency-demodulated using Temporal Fine Structure (TFS) since the robot's joint speed has a linear relationship with the frequency component. Then, the TFS of motor current is analyzed in TFR to get a normalized motion signal. Also, the raw signal is decomposed into basic segments and identified into different motion types through cosine similarity, providing total cycles of motion and number of motion types.

Secondly, Ordinal Pattern Analysis of Motor Current (OPAMC) is conducted where the identified signal in motion segmentation is synchronized with reference motion and Hilbert-transformed to get envelope for extracting ordinal patterns. The window parameter used in pattern extraction is based on physical interpretation since it is related to the robot's speed profile. Also, the probability distributions of ordinal patterns are compared between normal state and observed state through Jensen-Shannon Divergence (JSD).

Finally, in fault detection, the total JSD distributions are cross-validated among different joints and displayed on 3-dimensional feature space which is then reduced

to 1-dimension by Linear Discriminant Analysis (LDA).

For validation, the series of framework is tested on various operating conditions such as different velocity and payload to provide reliability on the study.

1.3. Thesis Layout

The thesis consists of following chapters: Chapter 2 reviews essential knowledge on fault characteristics of robot control system, signal processing and several types of statistical distance measure. Chapter 3 and 4 proposes robot diagnosis framework where Chapter 3 presents motion segmentation method based on Time-Frequency Representation (TFR) and Chapter 4 proposes Ordinal Pattern Analysis of Motor Current (OPAMC) for robot health assessment. Chapter 5 validates the proposed method with robot motion tests on different operating conditions. Finally, Chapter 6 summarizes contributions of the study and suggests future research scope.

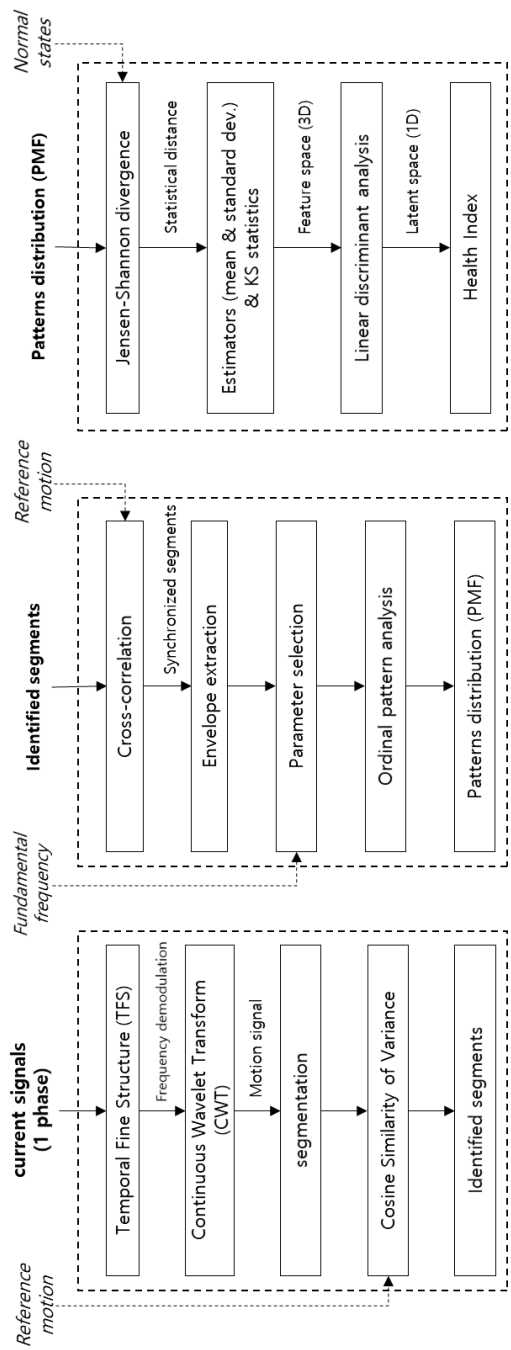

Figure 1-1. Diagnosis framework of robot's health assessment

Chapter 2. Literature Review

2.1. Robot system and malfunction

The main parts of robot system are sensor, controller, and manipulator. Compared to human system, sensor corresponds to the sensory nerves since it helps robot conscious to its surroundings, controller to brain since it is responsible for instructing the robot to act based on what it recognizes, and manipulator to body since it represents the actual motion.

Robot's manipulator is usually transmission-based actuation system, mainly consist of servo motor, speed reducer and timing belt in between. The servo motor has encoder that generates a train of pulses which can be used to determine position and speed of joints, and sometimes torque sensors. The different types of sensors in manipulator help controller measure the current behavior and transmit control signal to synchronize with desired behavior. When the manipulator has uncontrollable behavior such as backlash on speed reducer, the repeatability and accuracy of the robot's end-effector diminish [6] causing distortion in the control signal and the motor's input current.

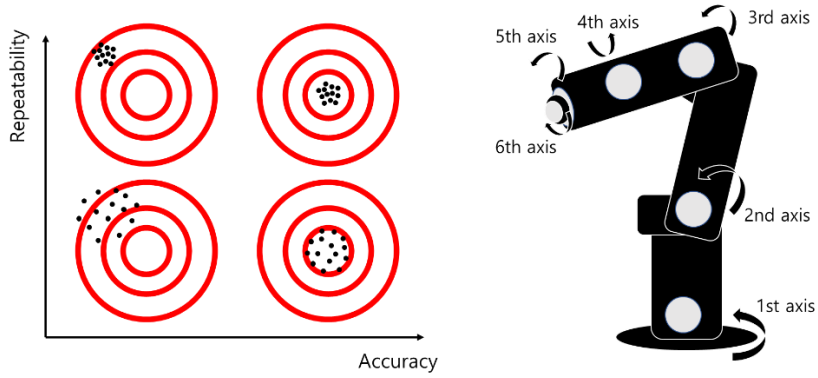

Figure 2-1. Performance test of robot system

(a) Repeatability and Accuracy (b)Vertically articulated robot

2.1.1 Closed loop control

To control robot's motion, user inputs desired behavior through a software, which is usually referred to as *teaching*. To carry out the teaching motion, the controller sends a control signal to the amplifier and the signal enters the motor in the form of an amplified current signal. The power of the motor is transmitted to the end-effector through robot's transmission system such as speed reducer and timing belt. Then, the robot's motion is adjusted through a closed loop control that feeds to the controller the error value between the desired behavior and the current robot behavior which is measured at the sensor unit [7].

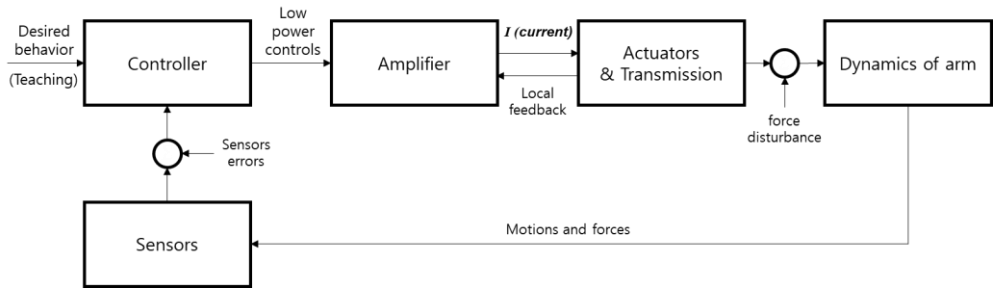

Figure 2-2. Diagram of closed-loop control [7]

2.1.2 Backlash of Strain Wave Gear

Typically referred to as Harmonic Drive, *Strain Wave Gear (SWG)* is a transmission system that reduces speed of motor by specific gear ratio and it is an essential component of robotic arm joint developed by W.Musser in 1955 [8]. The SWG is either cup style or pancake style, and consists of wave generator, flexspline and circular spline in common. Wave generator is a type of ball bearing with an electrical cam connected to the input shaft and rotates the flexspline, a flexible ring with gear teeth. The flexspline's gear is in conjunction with circular spline which has rigid ring gear forming a gear train [9].

The SWG is mainly used due to its characteristics such as high precision and gear ratio compared to cycloidal gear or planetary gear. However, cyclic loading and deformation of flexspline make it susceptible to the fatigue failure [10]. Also, failures such as gear tooth error increase tooth clearance between flexpline and circular spline resulting in backlash of the SWG and reduce the accuracy or repeatability of robot motion behavior [11].

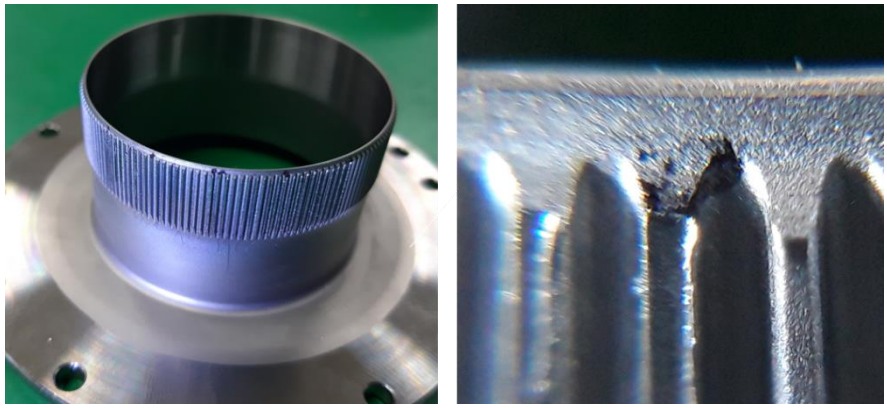

Figure 2-3. Flexspline and its failure

2.2 Continuous Wavelet Transform

Wavelet transform was first proposed by Norman Ricker (1940) for seismic wave analysis [12]. The wavelet transform could analyze almost all types of stationary and non-stationary signals compared to Fourier transform [13].

At first, Fourier Transform (FT) has been mainly used to analyze signal in frequency domain as it decomposes the entire signal into a frequency component. However, since it could only extract global frequency features using sinusoid function, local features of signal could not be extracted, and the analysis under varying speed conditions in which frequency characteristics changes over time had limitations.

In this context, Short Time Fourier Transform (STFT) was introduced by Gabor (1946) [14], in which time window was used to decompose the entire signal into segments and proceed the Fourier transform of segments to extract local features.

However, the same window length over all frequency components caused time-frequency resolution's compensation issue, and the local features on different frequency band could not be effectively extracted.

Continuous Wavelet Transform (CWT) presented by Grossman and Morlet (1980) is a Time-Frequency Representation (TFR) method which has overcome the limitations of STFT [15]. The STFT and CWT are similar in mechanism, however, as in Figure 2-4, the window length of CWT becomes narrower as the bandwidth of the frequency component increases and the adaptive time-frequency resolution facilitates analysis of non-stationary signal.

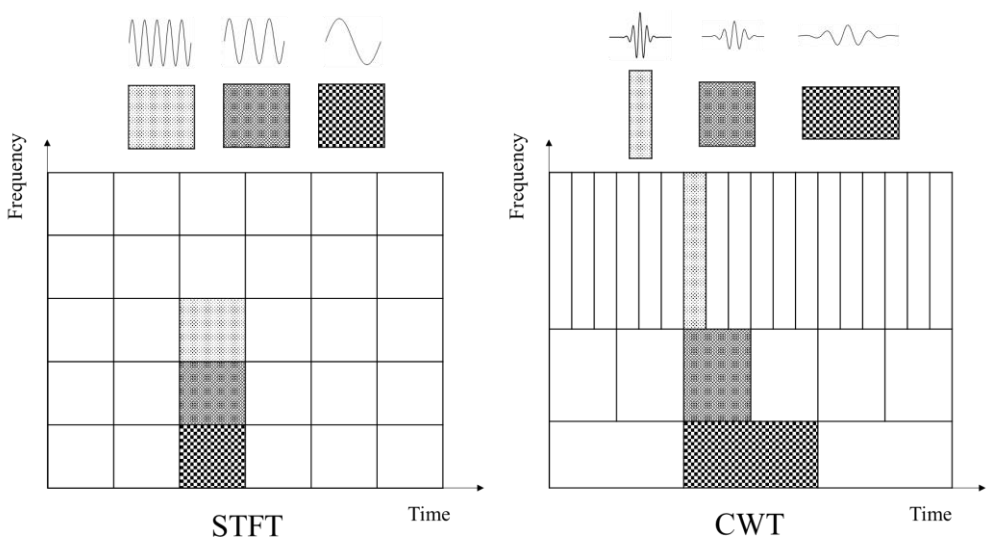

Figure 2-4. Comparison of time-frequency resolution between STFT and CWT

A CWT of a real signal $x(t)$ is defined as a set of convolutions with analyzing wavelet function $\psi(t)$ [16]:

$$CWT_x^{\psi}(a,b) = W(a,b) = \frac{1}{\sqrt{|a|}} \int x(t) \cdot \psi^* \left(\frac{t-b}{a} \right) dt \qquad (2\text{-}1)$$

where the signal $x(t)$ is decomposed into complex conjugates of the wavelet function $\psi^*(t)$ which is shifted and scaled in time [15]. Also, the wavelet basis function $\psi(t)$ is a window function or called as *kernel wavelet*. The a is a scale parameter and b is a time shift parameter or transition. $W(a,b)$ is wavelet coefficient corresponding to each a and b which is an inner product of signal $x(t)$ and kernel wavelet $\psi(t)$ scaled by energy normalization coefficient $1/\sqrt{a}$. To reproduce wavelet coefficient $W(a,b)$, the time t of kernel wavelet $\psi(t)$ is scaled by $1/a$ and time-shifted by b. As a kernel wavelet $\psi(t)$, *Morse wavelet* has been widely used since it is Gaussian-windowed sine wave and thereby scale parameter can be easily transformed into a frequency in CWT.

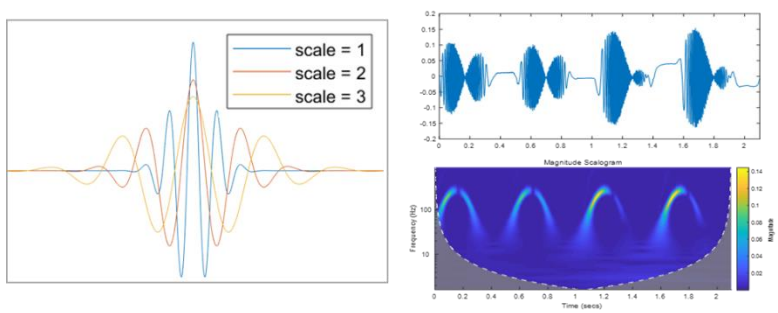

Figure 2-5. Continuous Wavelet Transform of input current

(a) Morse wavelet of scale 1,2,3 (b) CWT of 1cycle motion (4 segments)

CWT has been an effective tool since its adaptive feature facilitates extracting localized information regardless time and frequency resolution, and therefore, it has been implemented for signal processing method in system diagnostics. As an application in industry, wavelet-based features of mechanical and electrical faults have been implemented to diagnose induction motors at varying operating conditions [17].

2.3 Envelope and Temporal Fine Structure

Hilbert transform (HT) was first introduced to deal with a special case of integral equations in mathematical physics (Korpel, 1982) [18,19].

HT of the signal $x(t)$ is defined as (Hahn ,1996) [20]:

$$HT[x(t)] = \pi^{-1} \int_{-\infty}^{\infty} \frac{x(\tau)}{t-\tau} d\tau \tag{2-2}$$

The physical meaning of the equation is equivalent to a linear filter, where the amplitudes is fixed while the phase is shifted by $\pi/2$ [19]. HT can provide useful information about an amplitude, instantaneous phase, and frequency of vibrations and thereby it is an effective representation to describe the amplitude and frequency modulation of a time-series [20].

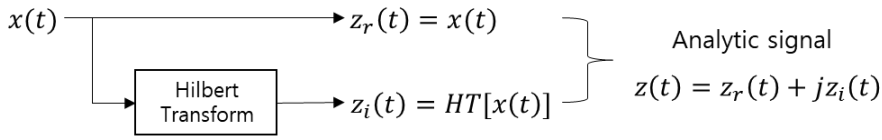

Figure 2-6. Analytic signal via Hilbert transform

1) Envelope $$a(t) = |z(t)| = \sqrt{z_r^2(t) + z_i^2(t)} \quad (2\text{-}3)$$

2) Instantaneous phase $$\emptyset(t) = \angle z(t) = arctan\left[\frac{z_i(t)}{z_r(t)}\right] \quad (2\text{-}4)$$

3) Temporal Fine Structure $$TFS = cos\emptyset(t) \quad (2\text{-}5)$$

Through HT, signal $x(t)$ is phase-shifted by π/2 and composes the real and imaginary part of analytic signal, respectively. Then, the amplitude of analytic signal offers the instantaneous amplitude, *envelope*, which is an effective signal processing method for an amplitude-modulated nature of the time-series. In addition, the phase of analytic signal, instantaneous phase, can describe time-varying frequency features in a way that the carrier signal from instantaneous phase, called *Temporal Fine Structure (TFS)*, can be used as a frequency demodulation method. Since the amplitude of TFS composed by sinusoidal functions fluctuates between -1 and 1, the TFS can be implemented as normalized phase representation.

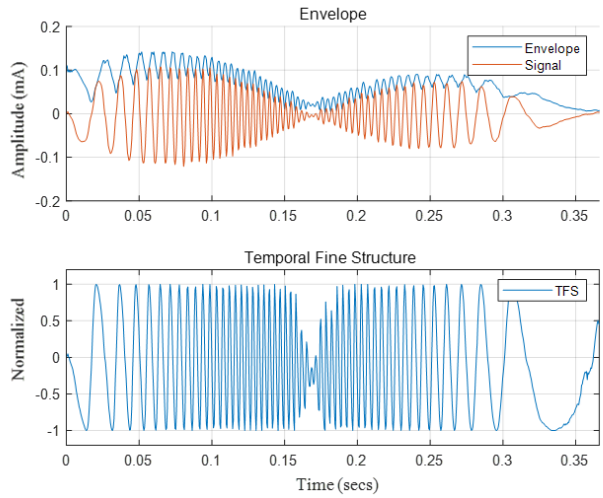

Figure 2-7. Envelope and Temporal fine structure

The envelope detector and TFS via HT can be as simple as lowpass filter, but it is highly precise and not sensitive to the carrier signal. The demodulation of signal amplitude and the extraction of instantaneous frequency can be applied in any oscillation signal, and thus, in any vibration unless it is highly impulse-modulated signal where the output of the demodulation is highly complicated to analyze [19].

In practice, the HT demodulation has been widely used in mechanical fault detection such as bearing and motor diagnostics. The envelope analysis has been the benchmark method for bearing diagnostics. Through envelope analysis, a signal is bandpass filtered in a high frequency band in which the structural resonance enhances the impulsive fault characteristics [21]. In addition, as to a motor diagnosis, Hilbert transform of stator-sampled current on motor current signature analysis (MCSA) has been proposed by R. Puche-Panadero and achieved detecting broken rotor bars at low slip or under no load [22].

2.4 Ordinal patterns

Ordinal pattern is the non-linear time series analysis which represents order relations of time series data. Through ordinal pattern analysis, the time series data can be decomposed and transformed into ordinal domain features, and this non-linear process can quantify the complexity of a system [23].

Considering a one-dimensional time series of length N, $Y = \{y_1, y_2, \dots, y_N\}$, vectors of α dimension are embedded by time lag τ, $V_t = \{y_t, y_{t+\tau}, \cdots, y_{t+(\alpha-1)\tau}\}$, and the number of embedding vectors that can be formed with X is $N - (\alpha - 1)\tau$.

An ordinal pattern of order α at time t with τ (also called permutation), $\pi_\alpha^\tau(t) = (r_1, r_2, \dots, r_\alpha)$ of $(1,2, \dots, \alpha)$ satisfies:

$$y_{t+r_1\tau} \leq y_{t+r_2\tau} \leq \cdots \leq y_{t+r_\alpha\tau} \tag{2-6}$$

where each vector's elements are sorted by increasing order. For order α, the number of ordinal patterns that can be formed is $\alpha!$. Also, when the element values are the same as $y_{t+r_{l-1}\tau} = y_{t+r_l\tau}$, the pattern orders are set to be $r_{l-1} < r_l$ for uniqueness [24].

For example, given a time series of:

$Y = \{1.41, 0.85, -0.11, -1.35, 1.77, 0.92, -1.92, 0.23, 1.77, -1.26, -0.79, 1.33, 0.14\}$, the permutation $\pi_5^2(3)$ is calculated from embedding vector observed to be $\{y_3, y_5 \dots, y_{11}\} = \{-0.11, 1.77, -1.92, 1.77, -0.79\}$. Since $y_7 < y_{11} < y_3 < y_5 = y_9$, the pattern order permutation is $\pi_5^2(3) = (r1, r2, r3, r4, r5) =$

(3,5,1,2,4). Also, the total number of embedding vectors is $11 - (5-1) * 2 = 3$ and the pattern types extracted are $5! = 120$.

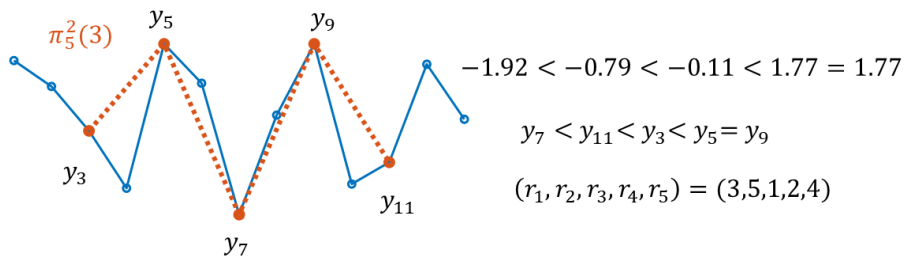

Figure 2-8. Extraction of ordinal patterns

Since the ordinal relations of signal rather than the values are compared, the ordinal patterns show robustness to impulse noise. Also, the distribution of ordinal patterns can represent the modulation of the signal as seen on Figure 2-9.

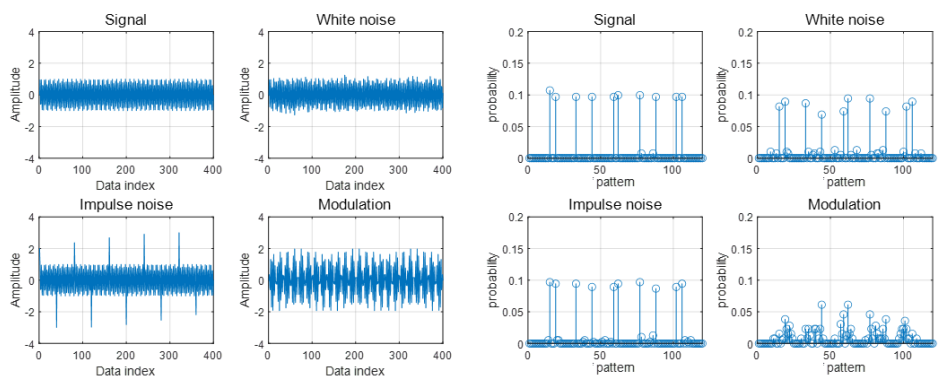

Figure 2-9. Time series and its ordinal pattern distribution with $N = 400$, $\alpha = 5$, $\tau = 2$

(a) sinusoidal signal (upper left) (b) white noise (upper right)
(c) impulse noise (lower left) (d) amplitude-modulated (lower right)

2.5 Measures of statistic distance

2.5.1 Jensen-Shannon divergence

Jensen-Shannon divergence (JSD) is one of method measuring the statistical distance between different probability distributions [25]. It came from Kullback-Leibler divergence (KLD) which measures the difference between distributions through information loss. However, since KLD is not symmetric, JSD takes advantage of mixture distribution to make it symmetric as shown below:

$$JS(p \parallel q) = \frac{1}{2}KL(p \parallel \chi) + \frac{1}{2}KL(q \parallel \chi) \tag{2-7}$$

$$\chi(x) = \frac{1}{2}\big(p(x) + q(x)\big) \tag{2-8}$$

$$KL(p \parallel q) = -\sum_{x} p(x) log\left(\frac{q(x)}{p(x)}\right) \tag{2-9}$$

The major feature in JSD is that the probability can be weighted at different values according to their importance so that it can provide a lot of advantages in decision problems. In addition, it is bounded to the Bayes probability of error and can be used as a true metric measure [26].

2.5.2 Kolmogorov-Smirnov statistics

Kolmogorov-Smirnov (KS) statistics is commonly used for goodness-of-fit test and defined as:

$$D_n = \sup_x |F_n(x) - F_{obs}(x)| \tag{2-10}$$

where $F_n(x)$ is the empirical cumulative distribution function of n-length reference data, and $F_{obs}(x)$ is that of observed data. The KS statistics means maximum value of the difference between two different empirical cumulative distribution functions. It is a measure of statistical distance where the value ranges between 0 and 1. The smaller the value of KS statistics, the greater the intersection of two different probability distribution functions (PDF). Thus, the separability of PDFs can be measured by analyzing KS statistics where the higher value means better separability. Figure 2-10,11 shows KS statistics between two different probability distributions. Assuming gaussian distribution and variance being the same, as the means get closer the KS statistics becomes smaller since the CDF distance of the two different distributions converges (Figure 2-10). In the same context, assuming the means being the same, the KS statistics becomes smaller when the difference of variance decreases (Figure 2-11). Also, the maximum value of KS statistics is 1 since probability and CDF range between 0 and 1.

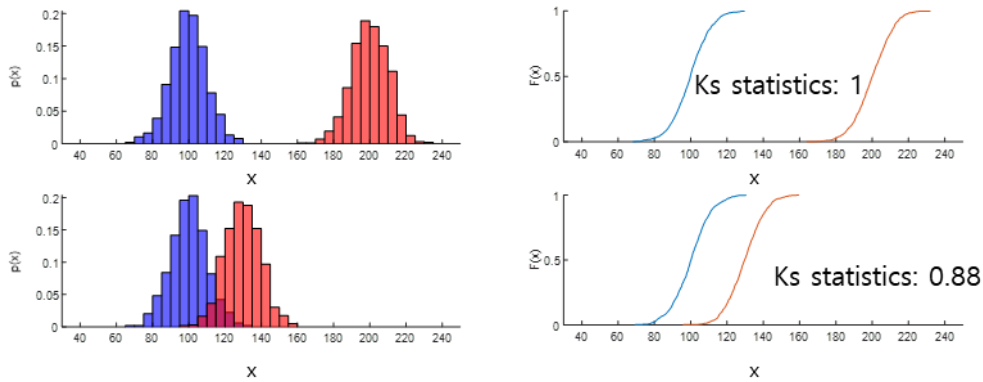

Figure 2-10. KS statistics compared with different means

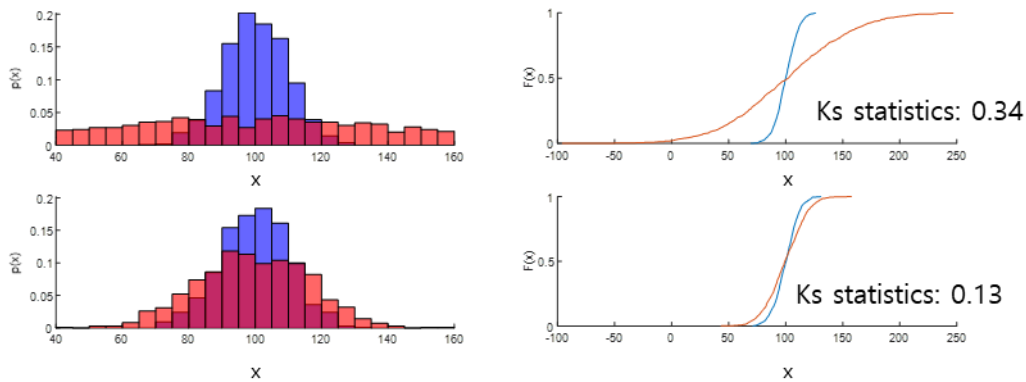

Figure 2-11. KS statistics compared with different variances

2.6. Linear Discriminant Analysis

Linear Discriminant Analysis (LDA) is a popular technique for dimension reduction and data classification. In LDA, through a linear transformation $P = \mathbb{R}^{r\times c}$, a r-dimensional x_i is mapped to a lower $c(<r)$-dimensional ξ_i through

$\xi_i = P^T x_i$ [27].

The LDA maximizes the ratio of between-class scatter matrix to within-class scatter matrix of data set in a way that the class separability is maximized [28].

In LDA, the between-class, within-class, and total-class scatter matrices are defined as [29]:

$$S_b = \sum_{k=1}^{K} n_k (m_k - m)(m_k - m)^T \tag{2-11}$$

$$S_w = \sum_{k=1}^{K} \sum_{x_l \in \pi_k} (x_i - m_k)(x_i - m_k)^T \tag{2-12}$$

$$S_t = \sum_{i=1}^{n} (x_i - m_k)(x_i - m_k)^T \tag{2-13}$$

where $m_k = \frac{1}{n_k} \sum_{x_l \in \pi_k} x_i$ is the class mean or class centroid of the k-th class, $m = \frac{1}{n} \sum_{i=1}^{n} x_i$ is the global mean or global centroid or total n points, and $S_t = S_b + S_w$.

According to the definition, the between-class S_b is maximized and S_w is minimized in the projected lower dimensional space, and thereby the objective function [29] in LDA optimization is as follows:

$$\underset{P}{\operatorname{argmax}} J = tr\left(\frac{P^T S_b P}{P^T S_w P}\right) \tag{2-14}$$

Chapter 3. Motion segmentation based on Time-Frequency Representation (TFR)

3.1 Fundamental frequency of motor current

When robot operates, the rotational speed fluctuates since the speed accelerates before it reaches the desired speed and slows down afterward as in Figure 3-1. The maximum rotational speed is reached within a short period of time, and the transient state overwhelms the steady state of robot motion. Therefore, it is necessary to analyze motor current assuming the robot behaves under varying speed condition.

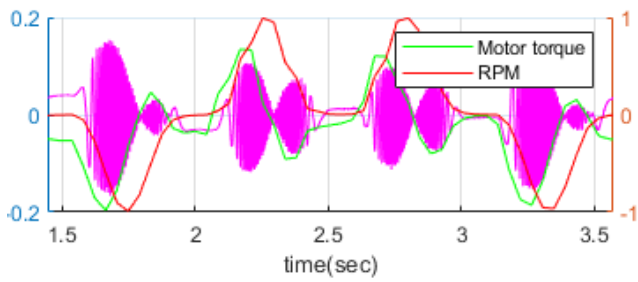

Figure 3-1. Control signal of motor torque and RPM aligned with motor input current

On transient state, modulation occurs in the amplitude and frequency of the current signal which can be observed through CWT. The CWT is a Time-Frequency Representation (TFR) method which helps to observe the accelerated motion in current signal and infer the robot joint's speed profile. Also, through the fundamental

frequency under varying speed condition, the maximum frequency observed in motor current is proportional to the maximum rotational velocity of robot motion. In Figure 3-2, a time-series robot motion signal is shown, and its CWT represents the fundamental frequency and provides robot's motion speed profile.

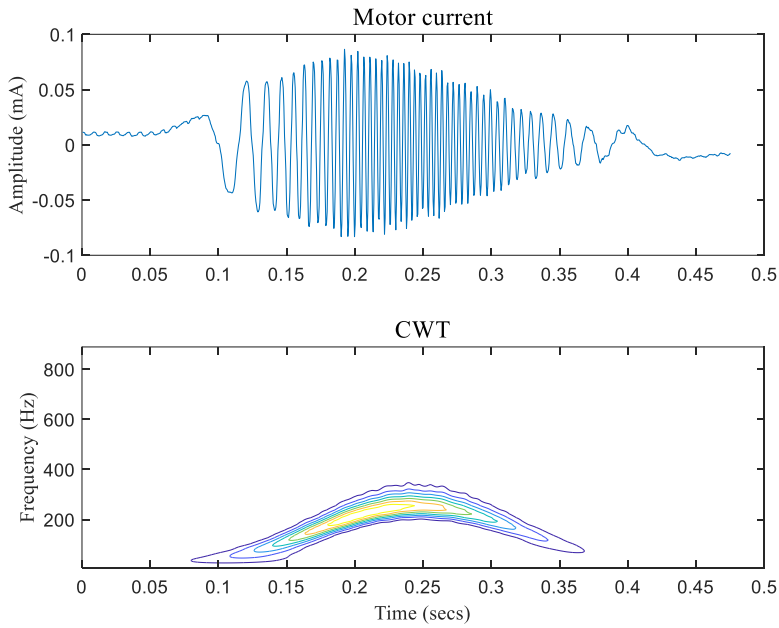

Figure 3-2. CWT and contour of fundamental frequency

3.2 Motion segmentation

Since robot works under varying speed conditions where speed increases and decreases near the desired value. The frequency modulation occurs with phase of current signal and it changes from low frequency to high frequency on the transient

state. Herein, Temporal Fine Structure (TFS) can be derived from instantaneous phase and used to demodulate the frequency components. The TFS is a carrier signal of instantaneous phase which ranges from -1 to 1 and extracts the frequency variation by means of normalized signal. In addition, the CWT of TFS (CTFS) is a time-frequency representation of TFS ranging from 0 to 1, and thereby can render normalized robot motion signal as in (3-1). When the robot's motion exists, the motion signal increases up to 1 which can be used for motion segmentation process.

$$S(t) = max(|CTFS(t,s)|) \ , \quad 0 \leq S(t) \leq 1 \qquad (3\text{-}1)$$

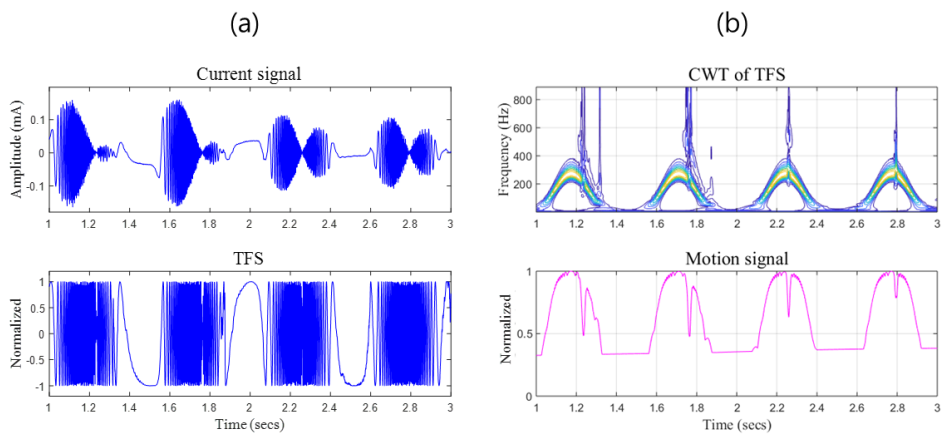

Figure3-3. Transformation of Temporal Fine Structure (TFS) to Motion signal

(a) Frequency demodulation (b) Motion signal through CTFS

3.3 Identification

Once segments of the signal are obtained, the identification process is necessary where the target segments are classified to which motion type it is corresponding to reference motion segments. Reference motion is a series of motion with at least 1 cycle, and the target motion is segmented the same number as the reference motion segments and identified. As sliding windows over target motion one segment by step with reference motion segments, motion similarity between target and reference segments is calculated. At this point, the reference and target segments are represented as the feature vector whose elements are the variance of each segments. The cosine similarity is calculated as follows:

$$sim^{(k)} = \frac{\vec{V}_r \cdot \vec{V}_t^k}{|\vec{V}_r||\vec{V}_t^k|} \quad \text{where } \vec{V}[s] = \frac{1}{N_s}\sum_{i=1}^{N_s}(x_i - \bar{x_s}) \qquad (3\text{-}2)$$

where $\vec{V}_r$ is a variance vector of reference motion, and $\vec{V}_t^k$ is a variance vector of target motion in *k*-th step of sliding window. Also, by shifting reference vector $\vec{V}_r$ across target vector $\vec{V}_t^k$, cosine similarity of *k*-th step, $sim^{(k)}$ is calculated resulting in repetition of cycle within robot motions as shown in Figure 3-4. Through this process, the total number of cycles and motion types in target motion can be known and help motion identified with the reference.

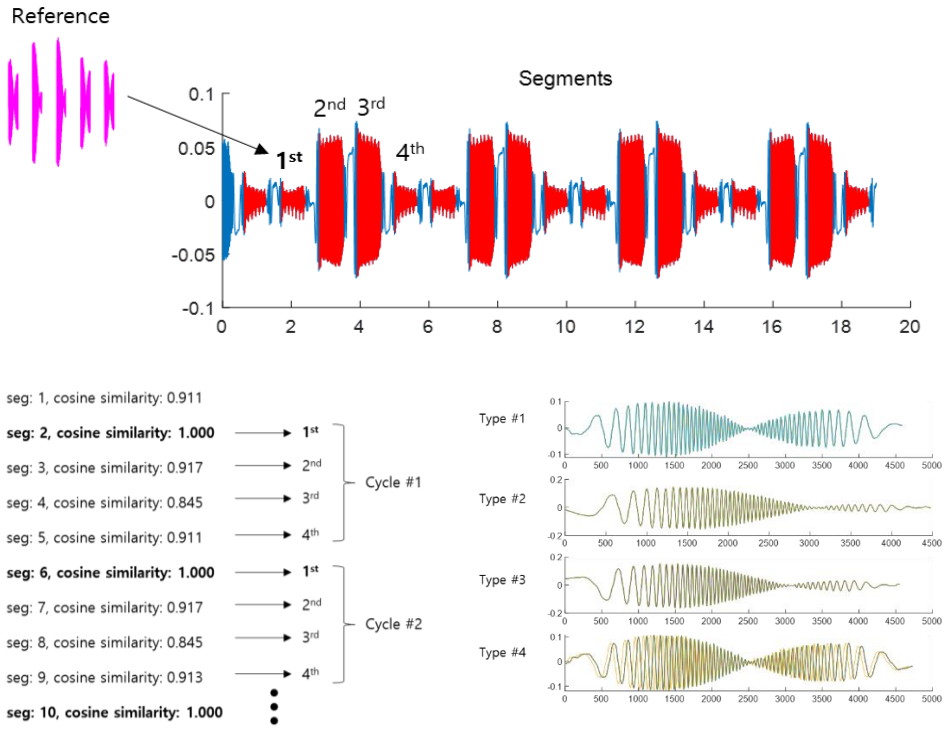

Figure3-4. Motion identification based on cosine similarity between reference and target segments

Chapter 4. Ordinal Pattern Analysis of Motor Current (OPAMC)

4.1 Preprocessing

4.1.1 Time synchronization

The identified segments need to be synchronized with reference in time since ordinal pattern analysis extracts relations in time domain. For this reason, cross-correlation is introduced for synchronization between reference and target motion segments.

Correlation is one of the commonly used method for similarity measure in matching process [30]. It is used for aligning two time series where one of the signals is delayed against the other. At the lag when the signal is best correlated, the cross correlation occurs highest and the signals line up [31].

In synchronization process, cross correlation between reference and target segments is defined as:

$$R(k) = \sum_{i=0}^{N-1} x_r(i)\, x_t(i-k) \tag{4-1}$$

where x_r and x_t are the segmented signal in reference and target motion respectively, and N is the smaller length in either reference or target signal.

In Figure 4-1, the time synchronization result shows that the target signal of normal and fault condition exactly correspond to reference motion signal.

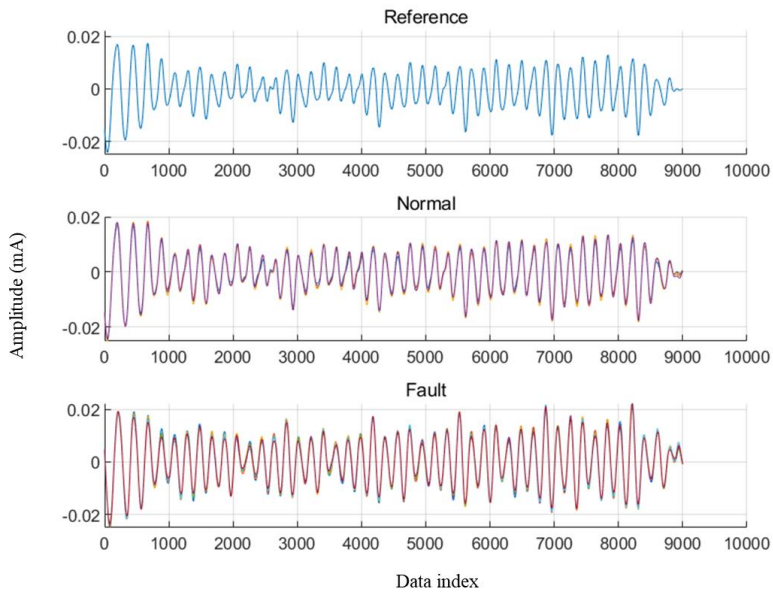

Figure4-1. Synchronization of target segments with reference.

4.1.2 Envelope extraction

The envelope of current signal corresponds to torque in motor current analysis, and thereby it can be a good indicator for its health assessment [22]. When backlash occurs in Strain Wave Gear (SWG), it reduces the robot performance of repeatability and accuracy leading to torque ripples in motor current [11]. Also, since the amplitude of motor input current represents the torque, the fault characteristics of

backlash can be demonstrated through its amplitude modulation which can be analyzed effectively through envelope analysis [22]. Therefore, in previous study, the motor current was once used for ball screw diagnosis in industrial robots (QiboYang and Xiang Li ,2020) [32], and the envelope of current signal was used to extract fault related features for unsupervised fault detection. (Fangzhou Cheng and Ajay Raghavan ,2019) [33].

In fact, the envelope obtained by Hilbert transform of motor current produces distinct differences in pattern among normal and fault joints as observed on Figure 4-2. In fault state, the envelope signal shows to be modulated in amplitude and frequency compared to normal state.

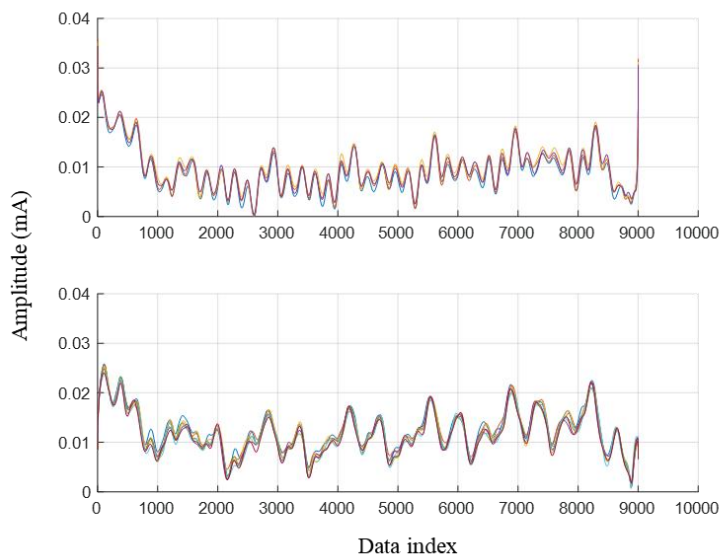

Figure4-2. Comparison of envelope between normal and fault axis.

4.2 Ordinal pattern distribution

The ordinal pattern can quantify the complexity of the dynamic system and extract the characteristic structure from the system [34] with strong advantage of noise robustness since it is not susceptible to impulse noise. Also, measuring current signal is physically less influenced by external noises than the vibration signal. As the rotational velocity increases, the transient state dominates the robot motion, and the non-linear analysis method of ordinal pattern performs better than Fourier transform which is a linear spectrum analysis method with constraints on constant speed condition. Furthermore, when fault occurs on robot joint, the dynamic instability and the reduction in repeatability make the ordinal pattern of envelope deviate from the normal state as the system dynamics property changes as in Figure 4-3.

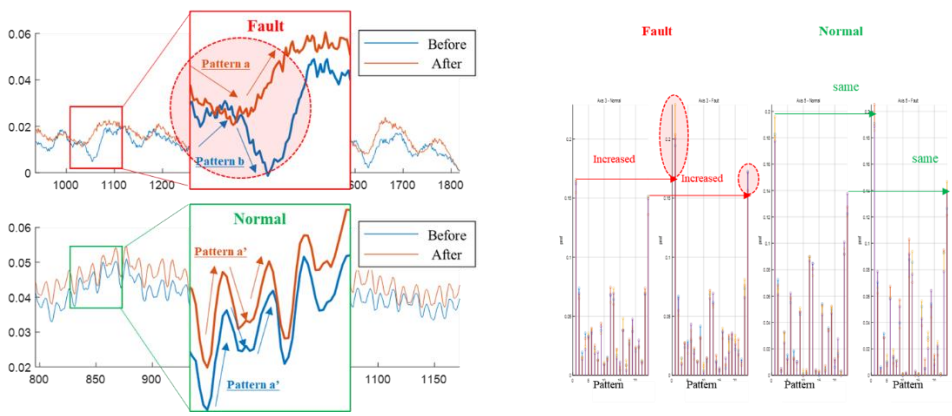

Figure4-3. Deviation of ordinal pattern distribution from normal to fault state.

(a) ordinal patterns in time series (b) Probability Mass Function (PMF)

4.2.1 parameter selection based on TFR

In ordinal pattern, setting the appropriate time delay parameter is critical since it decides spectral window applied in pattern extraction. The different time delay values can determine different pattern types to be extracted from the signal. In general, too low time delay is not able to capture the feasible fault characteristics from the signal. When the sampling frequency increases, the time delay parameter must set high in proportion for extracting the same ordinal patterns as previous low sampling frequency.

As seen in Figure 4-4, when the time delay parameter is set at low value as 1, the ordinal pattern distribution cannot effectively represent the differences in amplitude modulation. However, as the parameter increases from 1 to 3 in Figure 4-4b, the window is set long enough to extract modulation from the signal, and the following changes in ordinal pattern distribution can be observed. However, when the sampling frequency doubles in Figure 4-5, the same time delay value as in Figure 4-4 shows little divergence in ordinal pattern distribution of modulation signal. Therefore, the time delay parameter should increase from 3 to 6 in proportion to the change rate of sampling frequency to extract the same ordinal patterns as in previous low sampling frequency.

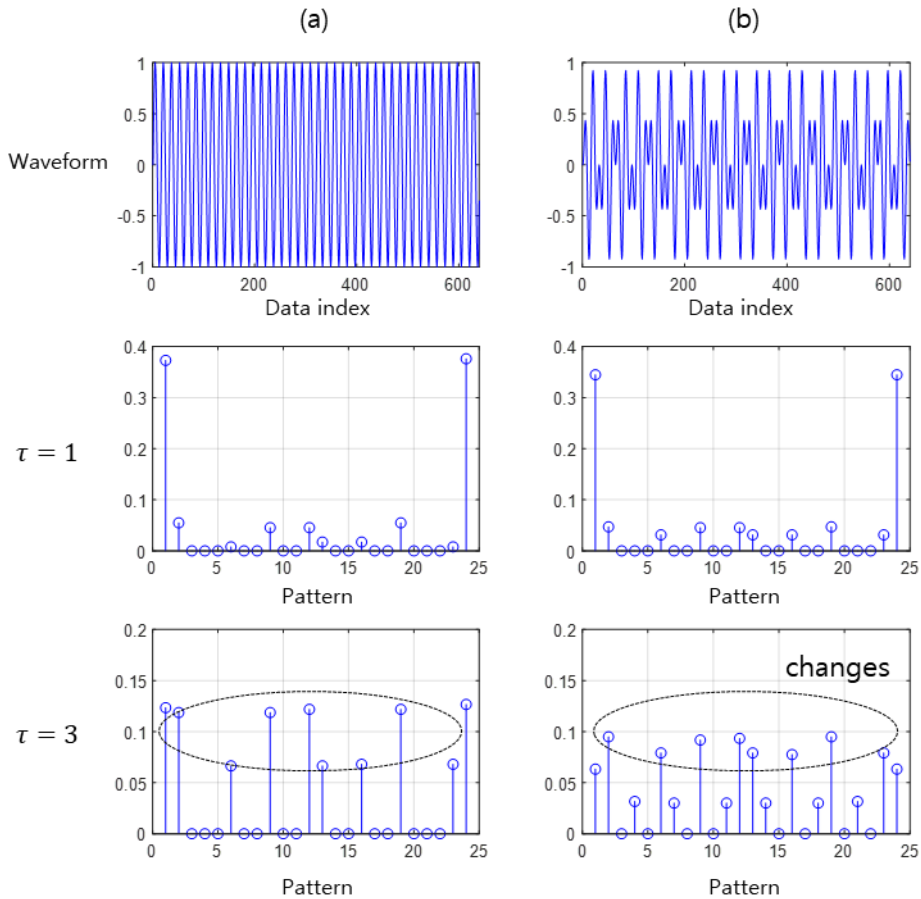

Figure4-4. Comparison of waveform and its amplitude modulation at sampling frequency F_s with respect to time delay (a) Sinusoidal (b) Modulation

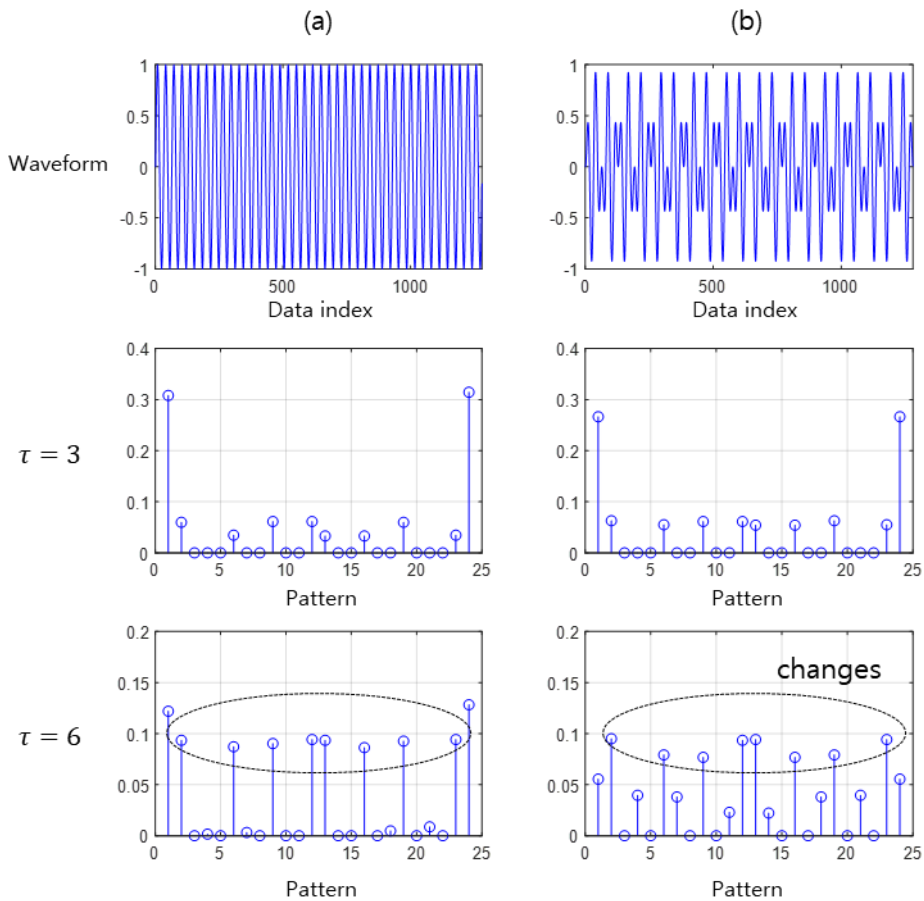

Figure4-5. Comparison of waveform and its amplitude modulation at sampling frequency $2F_s$ with respect to time delay (a) Sinusoidal (b) Modulation

Therefore, the optimal time delay parameter can be calculated through sampling frequency and fundamental frequency when extracting ordinal patterns that best represent the system.

The optimal time delay parameter τ_{opt} is:

$$\tau_{opt} = round(\frac{f_s}{f_{d,max} \cdot (\alpha - 1)} \cdot \gamma) \quad (4\text{-}2)$$

where f_s is the sampling frequency, $f_{d,max}$ is the maximum fundamental frequency in analyzing segments, and γ is the scale factor. The τ_{opt} increases in proportional to sampling frequency f_s , and decreases in proportional to pattern order α and maximum fundamental frequency $f_{d,max}$. Also, scale factor γ is a control parameter for adequate τ_{opt} values when either robot's maximum speed ($f_{d,max}$) or sampling rate (f_s) is too high or low.

In Figure 4-6, a single motion segment on time domain and its CWT are shown where the time window for extracting patterns is explained with fundamental frequency. The window is set to extract the smallest unit of modulation on maximum desired speed.

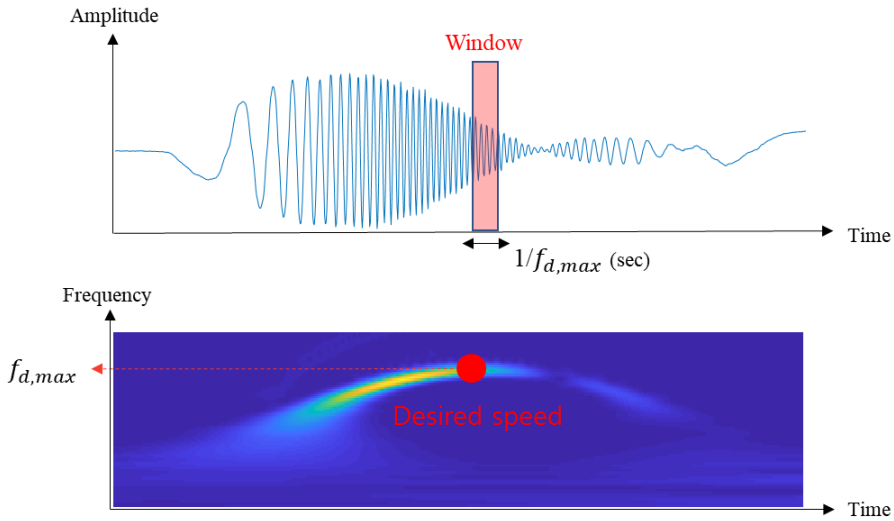

Figure4-6. Time window for extracting ordinal pattern

(a) Time series of segment (b) Fundamental frequency of desired speed

4.3 Fault detection

4.3.1 Jensen-Shannon divergence

Jensen-Shannon Divergence (JSD) can quantitatively measure the statistical distance between Probability Mass Functions (PMFs) since it is a symmetric metric. Also, the ordinal pattern distribution can be normalized into PMF, and the change of PMF can indicate health transition from normal to fault condition.

When a faulty reducer is mounted on robot joint, distinct difference in pattern distribution can be observed compared to the normal states. Since the distribution changes, the JSD of faulty-reducer distribution is observed to be higher than the normal one as in Figure 4-7.

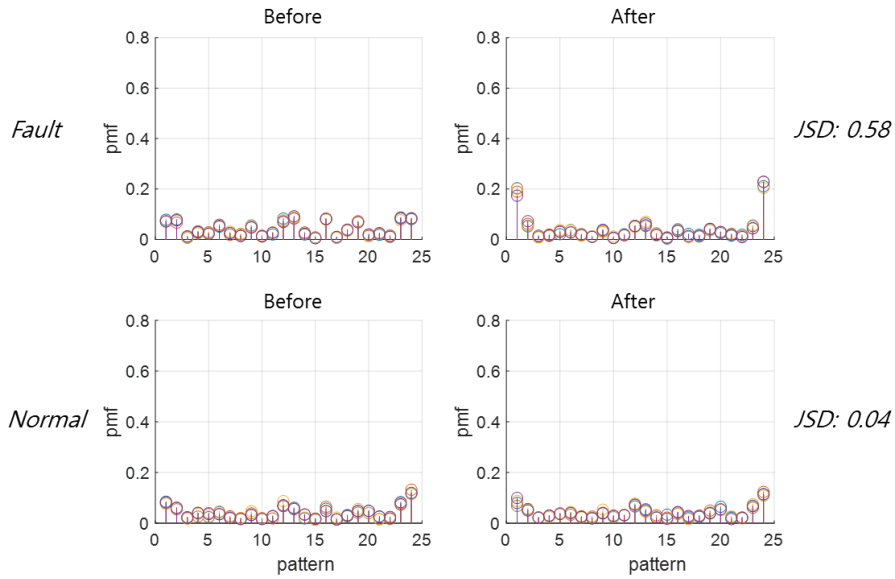

Figure4-7. Ordinal pattern distribution and its JSD before and after faulty SWG assembly (a) Before assembly on faulty axis (upper left) (b) After assembly on faulty axis (upper right) (c) Before assembly on normal axis (lower left) (d) After assembly on normal axis (lower right)

4.3.2 Distribution-based diagnosis

The histogram in Figure 4-8 represents JSD feature distribution compared between normal and faulty joint. JSD distribution assumed to be gaussian, sample mean and variance can be calculated through point estimation method. The change of these estimate can indicate how far the distribution of faulty state diverges from the normal state. In addition, Kolmogorov-Smirnov (KS) statistics can also measure separability in JSD distribution. In Table 4-1, the difference in parameter estimates

and KS statistics is represented where the fault axis experiences the increasing difference in mean and variance with increasing KS statistics as well. This suggests that the distribution shifts in position, and the shared area between normal and fault distributions lessens.

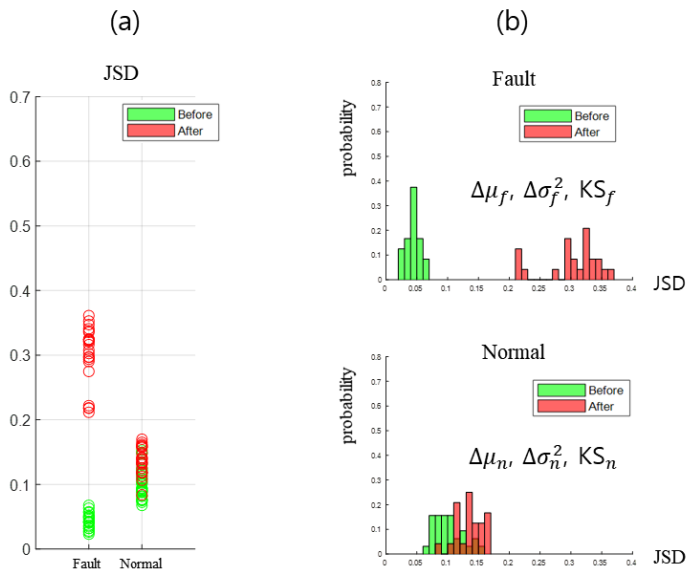

Figure4-8. Comparison of JSD distribution between normal and fault

(a) scatter plot (b) histogram

Table4-1. Statistical distance of normal and fault JSD distribution

	$\Delta\mu$	$\Delta\sigma^2$	KS statistics
Normal	14.7* e-03	3.23 * e-04	0.583
Fault	122* e-03	7.0 * e-04	1

The estimate difference and KS statistics between normal and fault axis are described on 3-dimensional feature space in Figure 4-9a. Through 3-dimensional space, the diverging characteristics of the features on fault axis can be observed. Also, by linear discriminant analysis, the 3D feature dimension can be reduced to 1 dimensional space to classify the robot's health states as in Figure 4-9b.

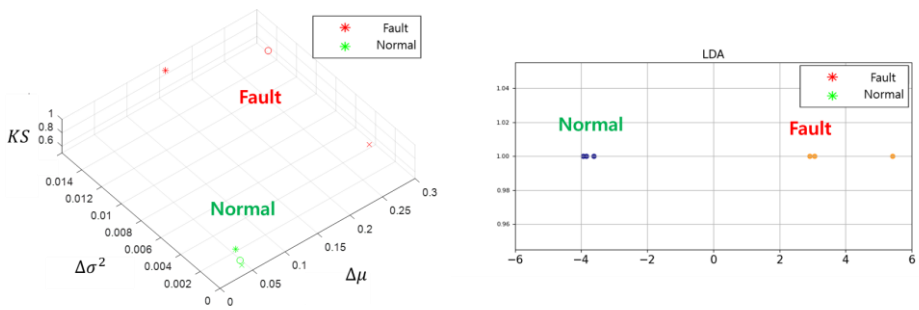

Figure4-9. Robot's health state on feature space

(a) 3D space of statistical feature (b) Projected 1D space through LDA

Chapter 5. Experiment and Validation

5.1 Experimental setup

In this experiment, we conducted motion tests on vertically articulated robot which consists of six axes as manipulator. For comparison between normal and fault axis, the robot was set to move one axis each per test. Then, the motor's three-phase input currents of all six axes were measured. The type of transmission used as a speed reducer was Strain Wage Gear (SWG) or commonly named, *Harmonic Drive*. For measuring current on six axes, the 18 channels of hall-effect current sensors were installed, and the sampling rate was set to be 2048Hz.

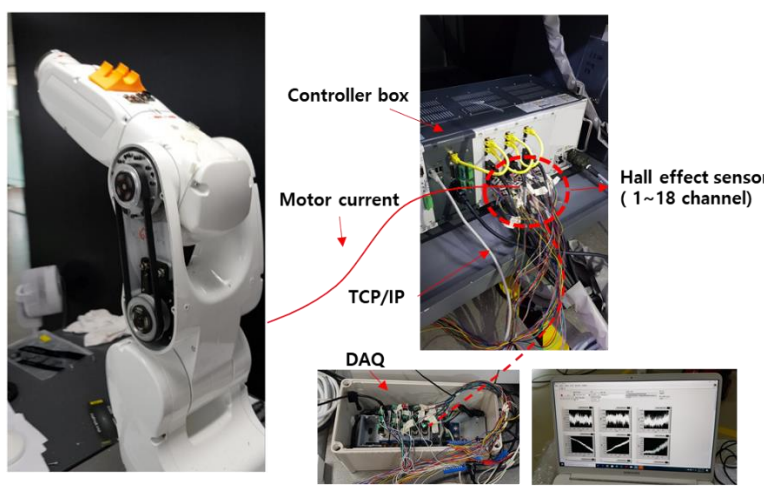

Figure5-1. Robot testbed for current measurement

As to failure in speed reducer, the SWG's flexspline was grinded a quarter of a perimeter and mounted on robot joint where the highest torque was created. In fact, the failure on reducer could demonstrate the backlash of robot and was difficult to perceive with human sense through vibration. Then, the normal joint was compared with faulty one.

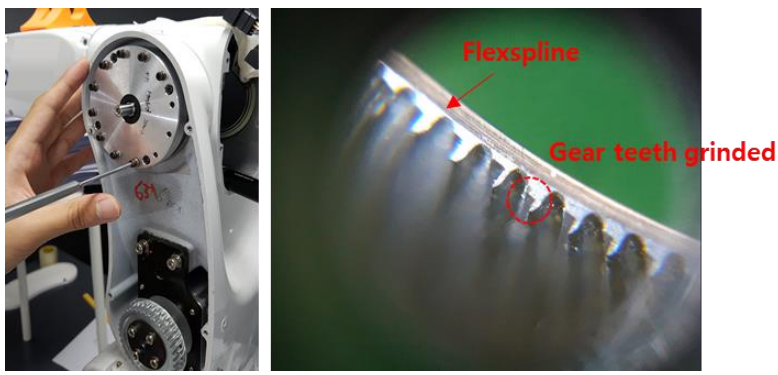

Figure5-2. Assembly of faulty Strain Wave Gear

(a) speed reducer on 3rd axis (b) Grinded teeth on flexspline

The experiment was conducted in two cases of control condition, varying joint's rotational speed or payload mounted on end-effector. The speed conditions were set at 20%, 50%, and 100% with no payload, and the payload conditions were changed to 0 kg, 1 kg, and 2 kg under the speed set at 100%. Also, in each case, the health condition of four motion cycles was analyzed before and after the assembly of faulty speed reducer. The JSD distributions of normal and faulty joint were analyzed with its estimate and KS statistics on 3- dimensional feature space, and processed dimension reduction through Linear Discriminant Analysis (LDA).

5.2 Experimental result

5.2.1 Case 1: Velocity 20, 50, 100%

The fundamental frequencies according to speed were observed to be 68 Hz, 157 Hz, and 314 Hz at speeds of 20%, 50%, and 100%, respectively. The same fundamental frequency was observed in different axis, and the frequency increased by approximately 31.4 Hz per 10% of speed.

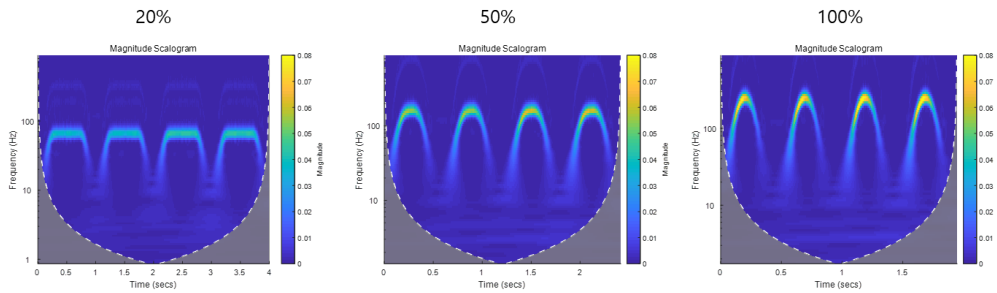

Figure5-3.CWT of 1 cycle motion and maximum rotational frequency of Velocity 20%, 50%, 100%

Table5-1. Fundamental frequency on different speed conditions

Velocity	Maximum frequency
20%	64Hz
50%	157Hz
100%	314Hz

(Payload: 0kg)

In OPAMC, window for ordinal pattern was set with different time delay parameter in each speed condition. Figure 5-4,5,6 shows JSD distributions of normal and fault axis with τ increasing from 1 to 25. The average values of each distribution were linked on black line over all τ values.

As a result, the JSD distribution shows distinct difference between normal and fault axis in all speed condition. The τ_{opt} value of which the distribution is separated at most decreases as the velocity increases. As the speed condition increases 20, 50, 100%, the τ_{opt} value decreases 15, 5 ,3. In other words, the desired speed through teaching increases and the maximum fundamental frequency increases, and therefore the modulation occurs at narrower window of signal and the τ_{opt} for extracting ordinal pattern decreases.

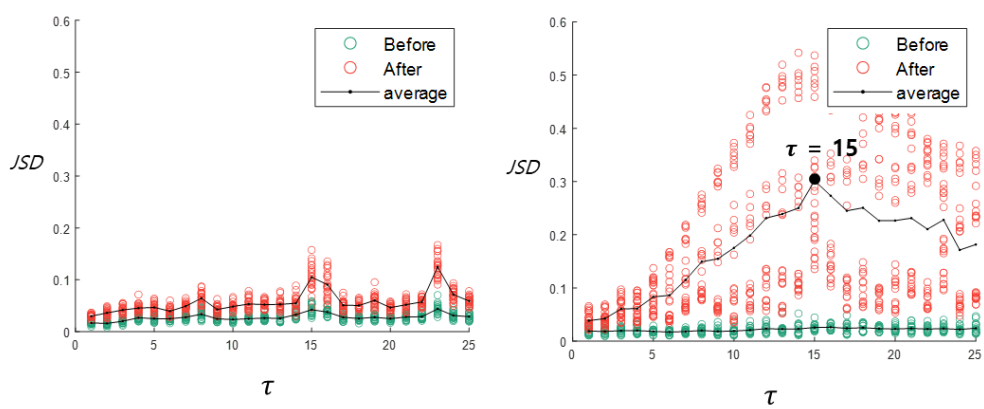

Figure5-4. Jensen-Shannon Divergence with different τ values
on 20% speed condition (a) Normal (b) Fault

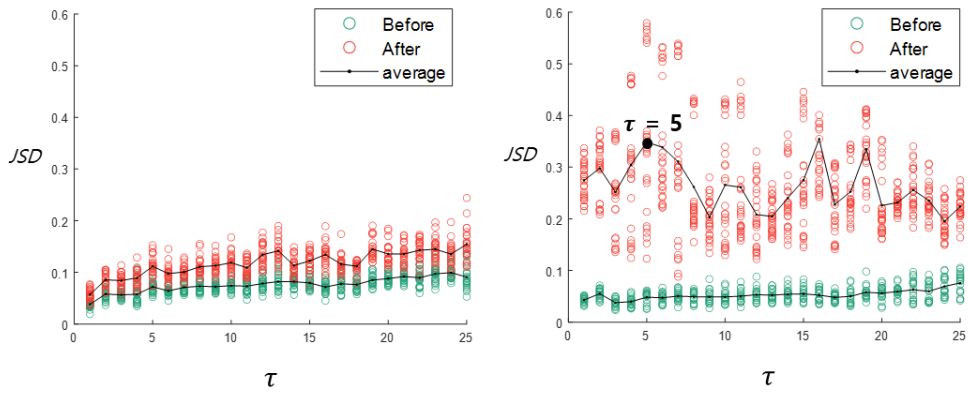

Figure5-5. Jensen-Shannon Divergence with different τ values on 50% speed condition (a) Normal (b) Fault

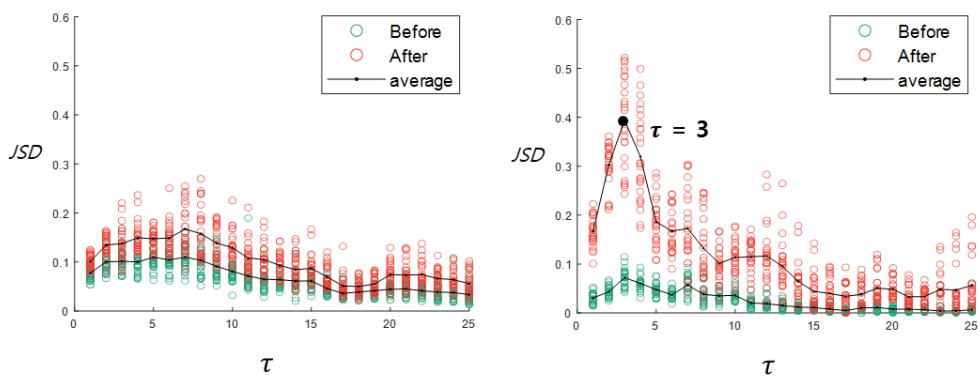

Figure5-6. Jensen-Shannon Divergence with different τ values on 100% speed condition (a) Normal (b) Fault

The result could be validated by applying same τ and comparing each other in all speed condition. Figure 5-7,8,9,10 represents PMF of ordinal patterns applying the same τ on speed condition of 20%, 100%. When τ is 3, only speed condition of 100% showed better distinction in PMF as JSD is 0.5955 after faulty SWG assembly compared to 0.1884 on normal condition. On the other hand, when τ is 15, only speed condition of 20% showed better distinction in PMF as JSD is 0.5770 after faulty SWG assembly compared to 0.1333 on normal condition. The τ_{opt} varies on different speed conditions, and too short or long window hardly extracts feasible ordinal patterns and catch modulation in signal.

Therefore, the τ_{opt} is dependent on robot's operating speed and can be calculated through its physical relation. The scale factor can be obtained as the actual τ_{opt} values are 15, 5, 3 on 20%, 50%, 100% respectively. The scale factor was 2, and the following τ_{opt} values on each speed condition were 14, 6, 4.

1) $\gamma = 1$

Velocity	20%	50%	100%
τ_{opt}	7	3	1

2) $\gamma = 2$

Velocity	20%	50%	100%
τ_{opt}	14	6	4

Table 5-2. Different scale factor and its τ_{opt} in each case

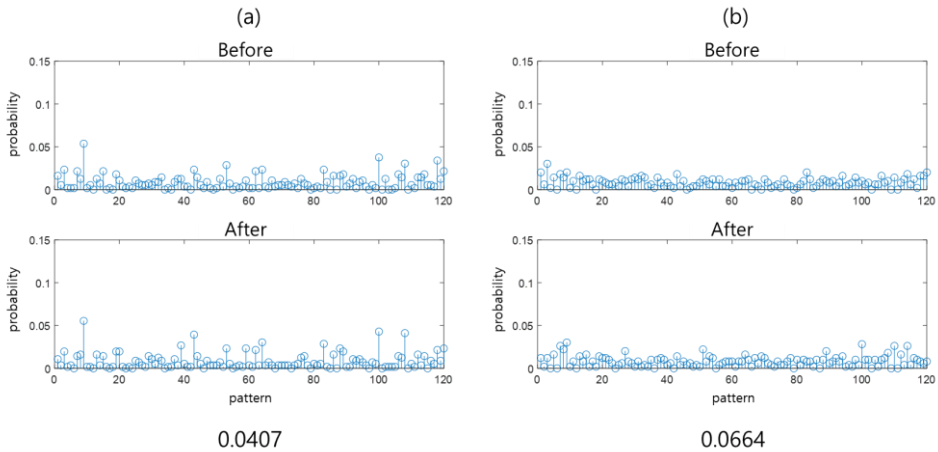

Figure5-7. Ordinal pattern distribution and its JSD with $\tau = 3$ on 20% speed condition

(a) Normal (b) Fault

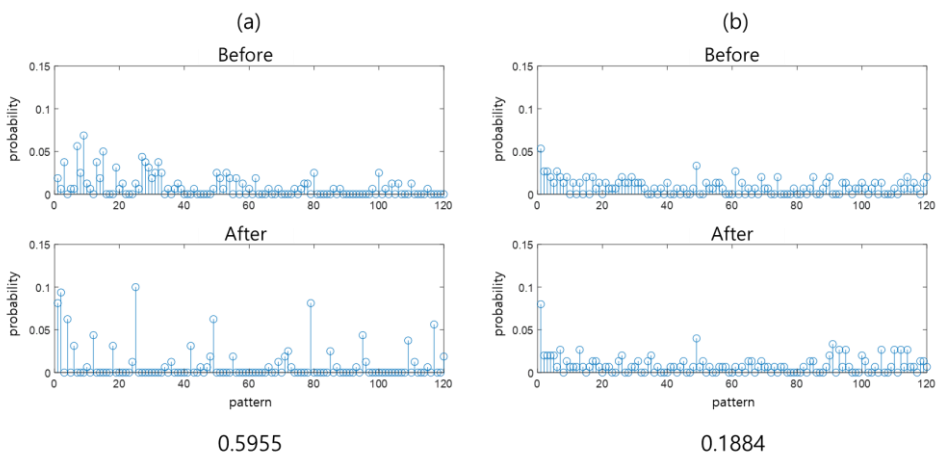

Figure5-8. Ordinal pattern distribution and its JSD with $\tau = 3$ on 100% speed condition

(a) Normal (b) Fault

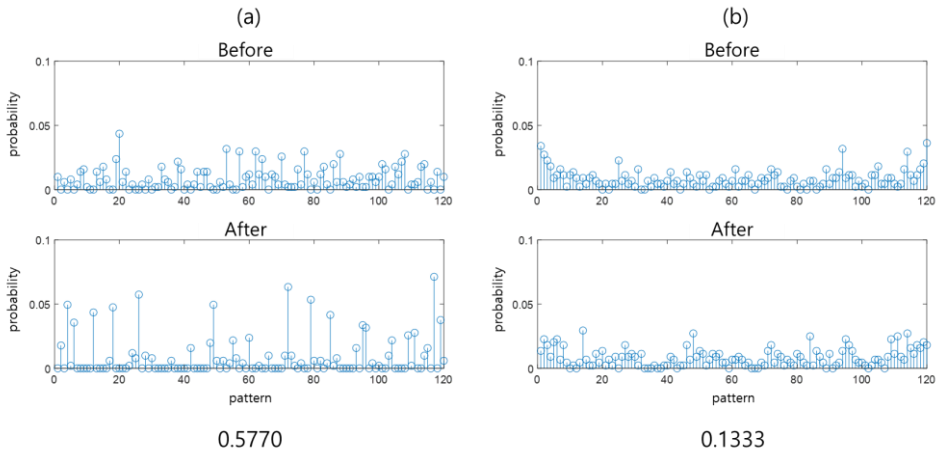

Figure5-9. Ordinal pattern distribution and its JSD with $\tau = 15$ on 20% speed condition

(a) Normal (b) Fault

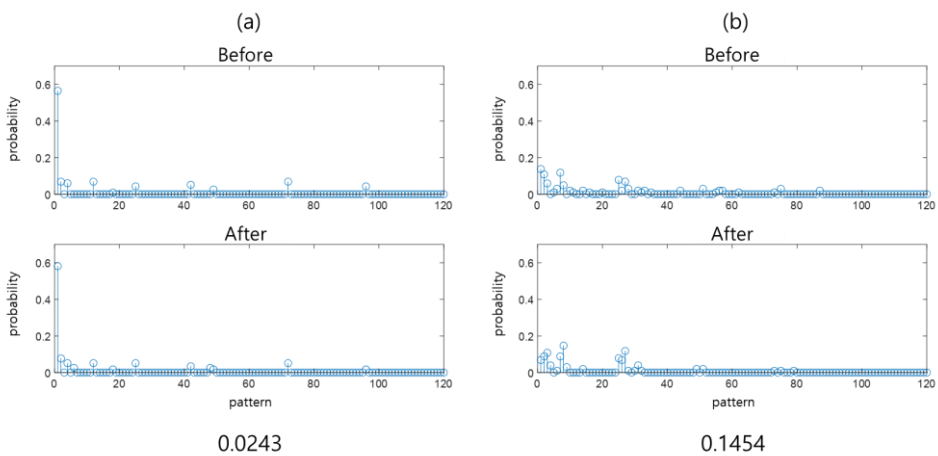

Figure5-10. Ordinal pattern distribution and its JSD with $\tau = 15$ on 100% speed condition

(a) Normal (b) Fault

On all speed condition with the each τ_{opt} values, the JSD is observed to be greater after the assembly of faulty SWG rather than the normal speed reducer mounted in Figure 5-11. Also, the JSD distribution of all motion segments is represented as histogram, and the distribution of the fault axis changes significantly after the assembly of faulty SWG in Figure 5-12.

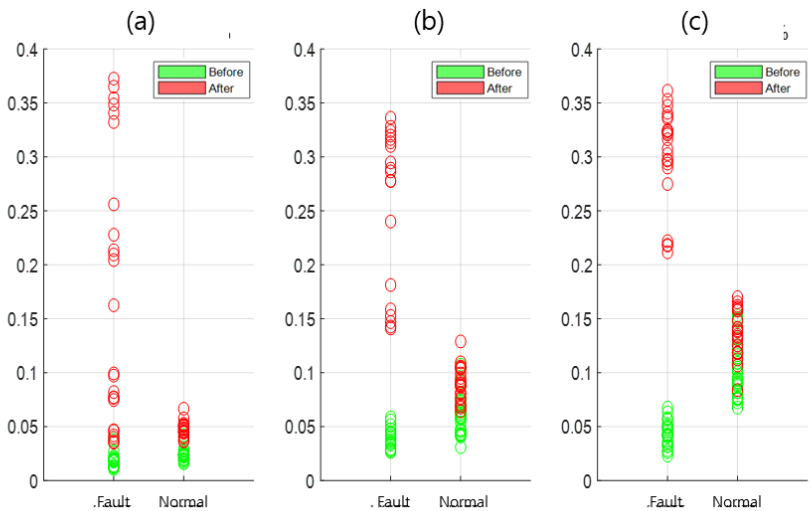

Figure5-11. JSD (scatter plot) on different speed conditions

(a) velocity 20% (b) velocity 50% (c) velocity 100%

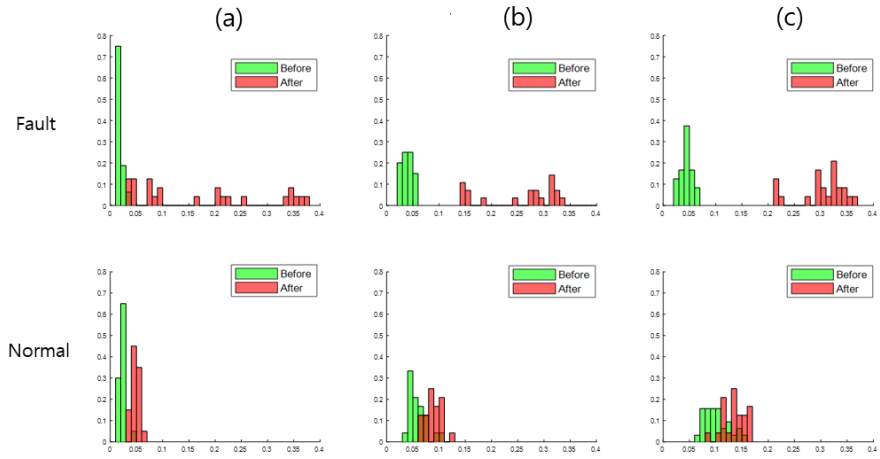

Figure5-12. JSD (histogram) on different speed conditions

(a) velocity 20% (b) velocity 50% (c) velocity 100%

In Figure 5-13,14, the order parameter α of 4 and 5 in OPAMC are compared and the distributions are displayed on 3-dimensional feature space through estimates of mean and variance assuming gaussian distributions, and KS statistics quantifying the separability between two different distributions in Table 5-2,3. Then, the 3-dimensional feature space is reduced to 1-dimensional latent space with LDA. As a result of the order increasing from 4 to 5, and the gap between normal and fault axis on the latent space became more distinct. This result appears to be the effect of increasing pattern complexity extracted with OPAMC as order of the ordinal pattern increases from 4 to 5.

Table5-3. Statistical distance and dimension reduction of OPAMC with $\alpha = 4$

Velocity		$\triangle \mu$	$\triangle \sigma^2$	KS statistics	LDA
20%	Normal	5.2* e-03	0.1* e-04	0.800	*-2.377*
	Fault	98.9* e-03	82* e-04	1	***1.797***
50%	Normal	10.1* e-03	0.6* e-04	0.777	*-2.414*
	Fault	177* e-03	114* e-04	1	***4.085***
100%	Normal	14.7* e-03	3.2* e-04	0.583	*-3.820*
	Fault	122* e-03	7.0* e-04	1	***2.730***

Table5-4. Statistical distance and dimension reduction of OPAMC with $\alpha = 5$

Velocity		$\triangle \mu$	$\triangle \sigma^2$	KS statistics	LDA
20%	Normal	24* e-03	0.2* e-04	0.950	*-3.620*
	Fault	154* e-03	160* e-04	0.938	***2.917***
50%	Normal	32* e-03	0.5* e-04	0.740	*-3.843*
	Fault	266* e-03	130* e-04	1	***5.420***
100%	Normal	35* e-03	1* e-04	0.642	*-3.937*
	Fault	258* e-03	20* e-04	1	***3.062***

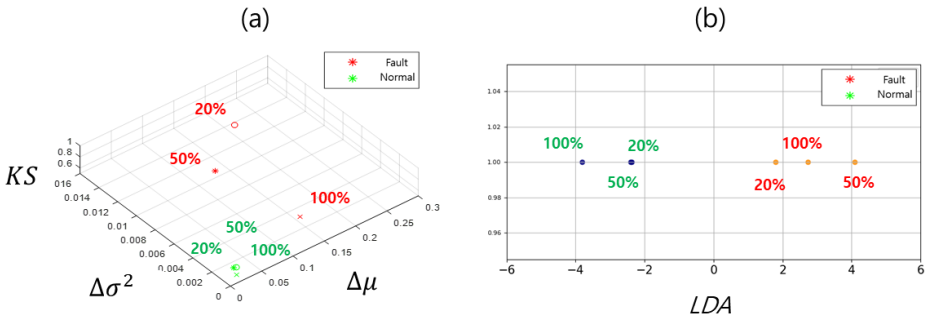

Figure5-13. Dimension reduction through LDA ($\alpha = 4$)

(a) Feature space (3D) (b) Latent space (1D)

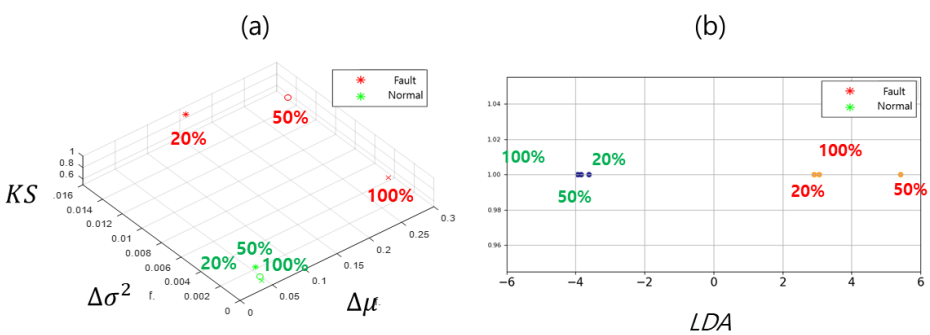

Figure5-14. Dimension reduction through LDA ($\alpha = 5$)

(a) Feature space (3D) (b) Latent space (1D)

5.2.2 Case 2: Payload 0,1,2kg

The payload being changed to 0,1 and 2 kg under the velocity set at 100%, the fundamental frequency was observed to be the same as 314 Hz in all payload conditions in Figure 5-15. The frequency was same in different joints since the operating velocity was set at same value. Also, the time delay parameter τ was set at 14 in all condition as the velocity was 100%.

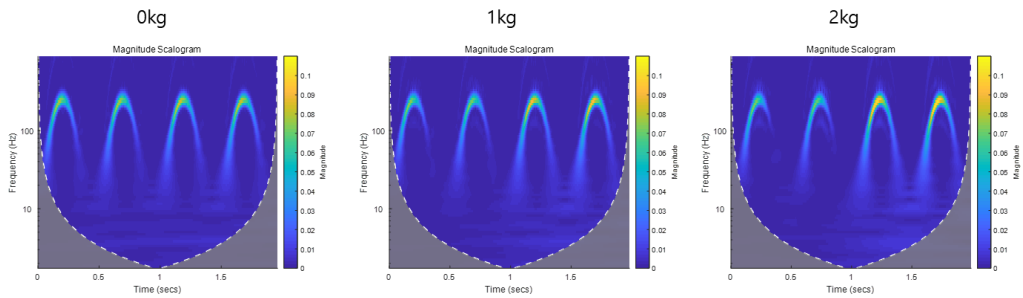

Figure5-15. CWT of 1 cycle motion and maximum rotational frequency of payload 0kg, 1kg, 2kg

Table5-5. Fundamental frequency on different payload condition

Payload	Maximum frequency
0kg	313Hz
1kg	314Hz
2kg	314Hz

(Velocity: 100%)

In Figure 5-16, the JSD of ordinal pattern distribution showed better distinction on fault axis and when there was no load on the joint. When increasing the order of the ordinal pattern, the similar result appeared as the velocity control condition, in which the backlash of the SWG is characterized more clearly when there was no load than load existing on end-effector.

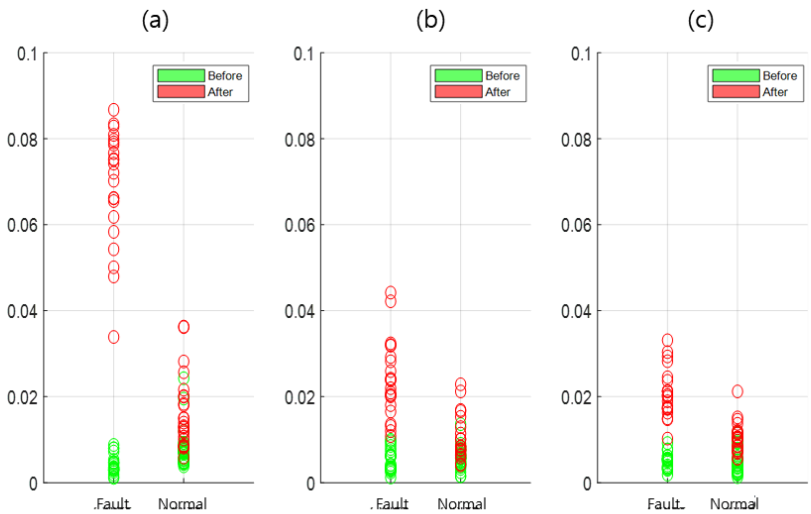

Figure5-16. JSD (scatter plot) on different payload conditions

(a) payload 0kg (b) payload 1kg (c) payload 2kg

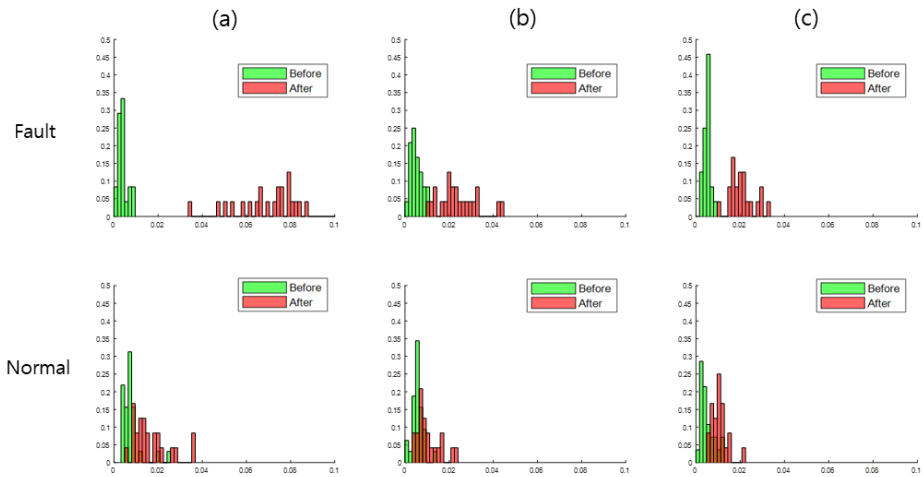

Figure5-17. JSD (histogram) on different payload conditions

(a) payload 0kg (b) payload 1kg (c) payload 2kg

In the same context as velocity control, the difference between before and after the assembly of faulty SWG could be seen more clearly when the JSD's distribution was represented as a histogram in Figure 5-17. It was better distinguished in faulty axis through the estimates and the KS statistics which represents the distribution divergence. In addition, through dimension reduction to one-dimensional latent space via LDA in Figure 5-18 and 19, the classification performance increased when the order α of ordinal pattern increased from 4 to 5. Similarly to velocity controls, the larger the order of the ordinal pattern is, the more capacity it is to represent the complexity of the pattern and make the distinction between normal and fault joints more pronounced as in Table 5-5,6.

Table5-6. Statistical distance between normal and fault after OPAMC with α=4

Payload		$\triangle \mu$	$\triangle \sigma^2$	KS statistics	LDA
0kg	Normal	8.6 * e-03	0.5 * e-04	0.692	***-2.417***
	Fault	121 * e-03	14.7 * e-04	1	***3.506***
1kg	Normal	4.8 * e-03	0.2 * e-04	0.547	***-4.834***
	Fault	22 * e-03	0.8 * e-04	0.957	***3.003***
2kg	Normal	5.3 * e-03	0.2 * e-04	0.680	***-2.432***
	Fault	33 * e-03	2.2 * e-04	1	***3.173***

Table5-7. Statistical distance between normal and fault after OPAMC with α=5

Payload		$\triangle \mu$	$\triangle \sigma^2$	KS statistics	LDA
0kg	Normal	29 * e-03	0.1 * e-04	0.792	***-6.230***
	Fault	160 * e-03	7.3 * e-04	1	***7.799***
1kg	Normal	20 * e-03	0.4 * e-04	0.759	***-8.453***
	Fault	50 * e-03	1.6 * e-04	1	***6.961***
2kg	Normal	22 * e-03	0.9 * e-04	0.920	***-8.338***
	Fault	53 * e-03	2.9 * e-04	0.957	***8.261***

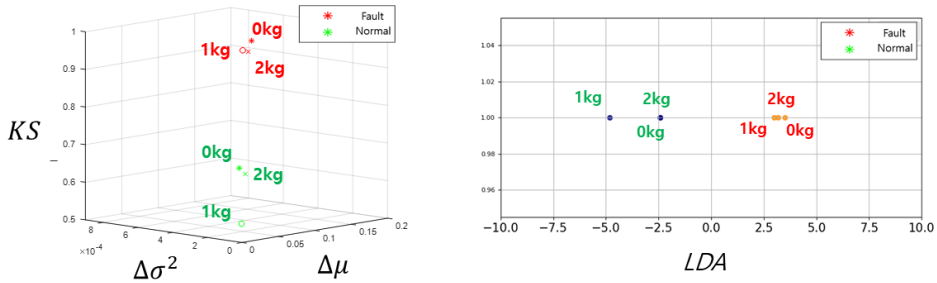

Figure5-18. Dimension reduction through LDA (α=4)

(a) Feature space (3D) (b) Latent space (1D)

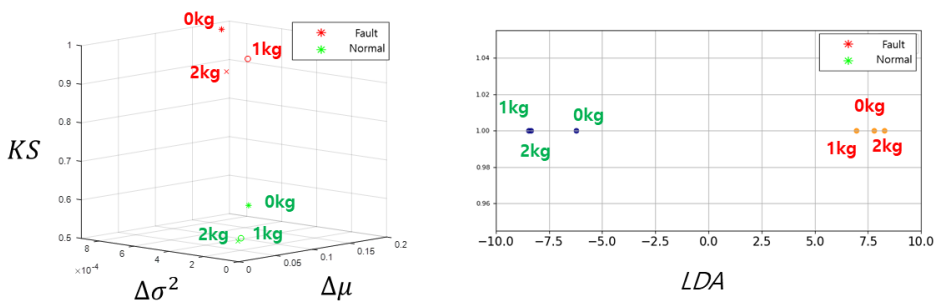

Figure5-19. Dimension reduction through LDA (α=5)

(a) Feature space (3D) (b) Latent space (1D)

Chapter 6. Conclusion

In this research, the robot diagnosis framework was proposed through several steps such as motion segmentation, OPAMC and distribution-based fault detection. Robot's motor input current was measured and segmented by a time-frequency technique which could represent the physical properties of the robot joint. Then, the ordinal pattern of the current's envelope signal was extracted, and the fundamental frequency was introduced for determining the time delay parameter τ_{opt}. Also, Jensen-Shannon Divergence (JSD) was suggested as a quantitative measure of health status with respect to the baseline of normal state. The JSD distribution was presented on 3-dimensional feature space with point estimates of gaussian model and KS statistics, and then the 3-dimensional feature space was reduced to 1-dimensional latent space via Linear Discriminant Analysis (LDA).

The series of diagnosis framework were validated on 2 cases of control condition, increasing rotational velocity and payload on the end-effector. The experimental result showed that the JSD distribution in faulty joint after OPAMC was distinctively different and separated from normal axis. Also, the payload on end-effector influenced the diagnosis performance as condition without payload showed better distinction in JSD distribution than the condition with payload.

6.1 Contribution and Future work

Overall, this study contributes to the health assessment of robotic arm joint in 3 aspects: 1) TFR-based approach of robot motion's segmentation and 2) parameter selection based on physical interpretation, and 3) the validation of framework on different operating conditions such as speed and payload. Also, 4) The distribution-based approach through comparative analysis gives a novel perspective compared to conventional method which has focused on concrete threshold that could be too subjective and dependent on personal experiences.

However, the limitation of this study is that only joints known to be susceptible have been tested and the order parameter in OPAMC has not been considered of other different values. In future study, experiments and verification with other joints and different types of robot are necessary as well as increasing order values of ordinal pattern with respect to its capability for extracting fault features.

Bibliography

[1] International Federation of Robotics Statistical Department. “World Robotics 2020 Industrial Robots report”, 2020

[2] B. Freyermuth, "An approach to model-based fault diagnosis of industrial robots," Proceedings. 1991 IEEE International Conference on Robotics and Automation, 1991, pp. 1350-1356 vol.2, doi: 10.1109/ROBOT.1991.131801

[3] Yunhan Kim et al. “Phase-based time domain averaging (PTDA) for fault detection of a gearbox in an industrial robot using vibration signals”, Mechanical Systems and Signal Processing, April. 2020, ISSN 0888-3270, vol.138, doi: 10.1016/j.ymssp.2019.106544

[4] Ali Rohan et al. "Rotate Vector (RV) Reducer Fault Detection and Diagnosis System: Towards Component Level Prognostics and Health Management (PHM)" Sensors, Nov. 2020, vol.20, no. 23: 6845. doi:10.3390/s20236845

[5] F. Cheng et al. "High-Accuracy Unsupervised Fault Detection of Industrial Robots Using Current Signal Analysis," 2019 IEEE International Conference on Prognostics and Health Management (ICPHM), 2019, pp. 1-8, doi: 10.1109/ICPHM.2019.8819374

[6] Hovland,G et al., ” Nonlinear identification of backlash in robot transmissions”, in ISR 2002 : Proceedings of the 33rd International Symposium on Robotics, pp. 1-6, Frankfurt, Germany, Oct. 7-11. 2002.

[7] Northwestern Robotics, Modern Robotics, Chapter 11.1: Control System Overview (Mar. 16,2018). Accessed: Mar. 20, 2021. [Online Video]. Available: https://www.youtube.com/watch?v=mGuDXlZEoSc&list=RDCMUCiK0J5wtnyX2jP-AiGbdhjg&index=20

[8] Walton, Musser C. "Strain wave gearing." U.S. Patent 2 906 143, Sep. 29, 1959

[9] Zhiyuan Yu, Jiawei Gong, “Introducing Kinematic Fundamentals of Strain Wave Gear for Robotic Arm Joint,” presented at the 2019 American Society for Engineering Education, Niagara Falls, NY, USA, April 12, 2019

[10] Jianlin Zheng, Wei Yang, “Failure Analysis of a Flexspline of Harmonic Gear Drive in STC Industrial Robot: Microstructure and Stress Distribution”, in 2018 IOP Conf. Ser.: Mater. Sci., vol. 452, Issue 4, doi: 10.1088/1757-899x/452/4/042148

[11] Bin Wang et al., “Measurement and analysis of backlash on harmonic drive,“ in 2019 IOP Conf. Ser.: Mater. Sci., vol.542. Xiamen, China, April 21-22, 2018

[12] N. H. Ricker, “The form and nature of seismic waves and the structure of seismograms,” Geophysics 1940, vol. 5, no. 4, pp. 348-366, Oct. 1940, doi: 10.1190/1.1441816

[13] S. A. A. Karim, M. H. Kamarudin, B. A. Karim, M. K. Hasan and J. Sulaiman, "Wavelet Transform and Fast Fourier Transform for signal compression: A comparative study," 2011 International Conference on Electronic Devices, Systems and Applications (ICEDSA), 2011, pp. 280-285, doi: 10.1109/ICEDSA.2011.5959031

[14] D. Gabor, “Theory of communication. Part 1: The analysis of information,” Journal of the Institution of Electrical Engineers - Part3: Radio and communication Engineering, vol. 93, no. 26, pp. 429-441, Nov .1946, doi: 10.1049/ji-3-2.1946.0074

[15] A. Grossmann, J. Morlet et al, “Decomposition of Hardy functions into square integrable wavelets of constant shape,” SIAM J. Math. Anal., vol. 15, no. 4, pp. 723–736, Sept. 1982, doi: 10.1137/0515056

[16] Avijit Chakraborty, David Okay, ” Frequency-time decomposition of seismic data using wavelet-based methods,” Geophysics 1995, vol. 60, no. 6, pp. 1906-1916, Dec. 1995, doi: https://doi.org/10.1190/1.1443922

[17] P. Gangsar, R.Tiwari, “Diagnostics of mechanical and electrical faults in induction motors using wavelet-based features of vibration and current

through support vector machine algorithms for various operating conditions," J Braz. Soc. Mech. Sci. Eng. , vol. 71, no. 2, pp. 71, Jan, 2019, doi: 10.1007/s40430-019-1574-5

[18] A. Korpel, "Gabor: frequency, time, and memory," Appl. Opt., vol. 21, no. 21, pp. 3624-3632 Oct. 1982, doi: 10.1364/AO.21.003624

[19] M. Feldman, "Hilbert transform in vibration analysis," Mechanical Systems and Signal Processing 25 (2011), vol. 25, no. 3, pp. 735-802, doi: 10.1016/j.ymssp.2010.07.018

[20] S.L. Hahn, Hilbert transforms in signal processing, Artech House, Inc., Boston, 1996.

[21] R. B. Randall, J. Antoni , "Rolling element bearing diagnostics—A tutorial," Mechanical Systems and Signal Processing , vol. 25, no. 2, pp. 485-520, Feb. 2011, doi: 10.1016/j.ymssp.2010.07.017

[22] R. Puche-Panadero et al., "Improved Resolution of the MCSA Method Via Hilbert Transform, Enabling the Diagnosis of Rotor Asymmetries at Very Low Slip," in IEEE Transactions on Energy Conversion, vol. 24, no. 1, pp. 52-59, March 2009, doi: 10.1109/TEC.2008.2003207.

[23] K. Keller, M. Sinn, "Ordinal analysis of time series," Physica A: Statistical Mechanics and its Applications, vol. 356, no. 1, pp. 114-120, 2005, doi: 10.1016/j.physa.2005.05.022

[24] Jing Wang et al., ”Dissimilarity measure based on ordinal pattern for physiological signals,” Communications in Nonlinear Science and Numerical Simulation, vol. 37, pp. 115-124, 2016, doi: 10.1016/j.cnsns.2016.01.011

[25] Cover, T.M., Thomas, J.A.: Elements of Information Theory. Wiley, New York, NY (1991)

[26] J. Lin, "Divergence measures based on the Shannon entropy," in IEEE Transactions on Information Theory, vol. 37, no. 1, pp. 145-151, Jan. 1991, doi: 10.1109/18.61115.

[27] Wang H., Ding C., Huang H. (2010) Multi-label Linear Discriminant Analysis. In: Daniilidis K., Maragos P., Paragios N. (eds) Computer Vision – ECCV 2010. ECCV 2010. Lecture Notes in Computer Science, vol. 6316. Springer, Berlin, Heidelberg. doi: 10.1007/978-3-642-15567-3_10

[28] S. Balakrishnama, A. Ganapathiraju, “Linear Discriminant Analysis—A Brief Tutorial”, Institute for Signal and Information Processing, Mississippi State Univ. vol. 11, Jan. 1998

[29] Fukunaga, K. (1990). Introduction to Statistical Pattern Recognition-Second Edition.

[30] Feng Zhao et al., "Image Matching by Normalized Cross-Correlation," 2006 IEEE International Conference on Acoustics Speech and Signal

Processing Proceedings, 2006, pp. II-II, doi: 10.1109/ICASSP.2006.1660446.

[31] William Menke, Joshua Menke, in Environmental Data Analysis with MatLab, 2012

[32] Qibo Yang et al., “Fault Diagnosis of Ball Screw in Industrial Robots Using Non-Stationary Motor Current Signals,” Procedia Manufacturin, vol. 48, pp. 1102-1108, 2020, doi: 10.1016/j.promfg.2020.05.151

[33] F. Cheng et al., "High-Accuracy Unsupervised Fault Detection of Industrial Robots Using Current Signal Analysis," 2019 IEEE International Conference on Prognostics and Health Management (ICPHM), 2019, pp. 1-8, doi: 10.1109/ICPHM.2019.8819374

[34] K. Keller, M. Sinn, “Ordinal analysis of time series,” Physica A: Statistical Mechanics and its Applications, 2005, vol. 356, no. 1, pp. 114-120, 2005, doi: 10.1016/j.physa.2005.05.022

요약(국문 초록)

산업용 로봇은 스마트 팩토리의 보급에 따라 많은 산업 분야에 걸쳐 사용되고 있으며, 그 수요는 지속적으로 늘어나고 있는 추세이다. 복잡한 자동화 공정 라인들의 의존성으로 인해 한 라인의 고장은 커다란 경제적 손실을 야기할 수 있고, 이에 따라 로봇의 건전성 진단은 중요한 이슈로 자리잡았다.

산업용 로봇은 크게 센서부, 제어부, 구동부로 이루어져 있으며, 구동부의 핵심 부품인 스트레인 웨이브 감속기는 모터의 동력을 엔드 이펙터로 전달해주는 기능을 하게 된다. 하지만 감속기의 주요 구성요소인 플렉스플라인은 피로파괴가 잘 일어나며, 이에 따라 백래쉬 현상이 일어나는 문제를 보인다. 기존에 로봇의 건전성 진단을 위한 많은 방법이 소개되었지만 1) 역학적 모델의 근사화 과정에서 불확실성이 존재하였고, 2) 진동신호는 외부 노이즈 영향을 많이 받았으며, 3) 물리적 설명 및 모션 전처리 과정이 부족하다는 단점을 보였다.

따라서 본 연구에서는 로봇의 축에서 상대적으로 물리적인 외부 영향을 덜 받는 전류신호를 측정하여 로봇의 건전성을 분석하였다. 또한 물리적 해석에 기반하여 진단 프레임워크를 구성하였고, 각 단계는 1) 로봇 모션 분리, 2) 모터 전류의 서수패턴 분석 (OPAMC), 3) 통계적 고장 진단으로 설명된다. 처음으로, 모션 분리 단계에서는 축의 회전 속도에 비례하여 전류신호의 주파수 변조가 일어나는 점에 착안해 신호의 시주파수 분석을 진행하였고, 정규화 모션 신호를 이용해 로봇의 작동 구간을 나누었다. 또한 모션 레퍼런스와의 코사인 유사도를 이용하여 모션

식별 과정을 진행하였고, 총 작동 사이클을 계산하고 모션 타입을 분류하였다. 두번째 OPAMC 단계에서는 레퍼런스 모션에 시간 동기화된 신호를 힐버트 변환 및 포락 신호를 구하였고, 운행 상태에 기반한 기본 주파수를 이용하여 최적 파라미터를 이용하여 서수 패턴을 추출하였다. 또한 특정 축에 대하여, 정상 상태 및 관찰 대상의 서수패턴을 확률 질량 분포로 나타내었으며 그 차이를 Jensen-Shannon Divergence (JSD)으로 계산하여 서수패턴의 분포가 정상 상태에 기반하여 얼마나 변화했는지 정량적으로 나타내었다. 마지막으로, 확률적 고장 진단 단계에서는 앞서 계산된 JSD 분포를 잘 나타낼 수 있는 통계적 추정치를 이용하여 고장 감속기가 결합된 축과 정상 축을 특징인자 공간에서 구별하였고, 차원 축소를 진행하여 1차원 공간에서 정량적으로 나타냈다.

실험은 2가지 운행조건의 통제를 통해 검증되었는데, 로봇 축의 속도를 20,50,100%로 증가하였고, 페이로드를 0, 1, 2kg로 증가시키며 고장 및 정상축을 비교해보았다. 결과적으로 속도가 증가함에 따라 축에 관계없이 기본주파수가 동일하게 비례하여 증가하는 것을 관찰할 수 있었고, 분해결합 전후로 고장 축에서 서수패턴 분포의 JSD가 더 큼을 볼 수 있었다. 또한 모든 속도조건에서 정상축 및 고장축의 JSD 분포 차이가 확연히 구별되는 것을 볼 수 있었다. 페이로드의 통제 조건에서는 엔드 이펙터에 부하가 존재하지 않을 때 정상 및 고장축이 확연히 구별되는 것을 관찰할 수 있었다. 이는 페이로드가 없을 때 상대적으로 축에 걸리는 토크의 변조가 컸고, 감속기의 백래쉬가 신호의 서수 패턴에 더 선명히 드러남을 의미했다.

본 연구에서는 모션 분리 및 서수패턴 분석 기법과 이에 필요한 최적 파라미터를 제안함으로써 고장 진단 프레임워크을 구성하였다. 여기서

분포에 기반한 결함 진단은 로봇 고장을 판단하는 기준이 모호하다는 점에 착안했을 때, 축 간 비교 분석 등을 통해 더욱 효과적으로 진단할 수 있음을 의미하였다. 또한 이러한 일련의 과정은 속도 및 페이로드 등 다양한 운행조건에서 검증됨으로써 신뢰성이 높은 결과를 도출했다는 점에서 그 의의가 있다고 볼 수 있다.

주요어 : 산업용 로봇
스트레인 웨이브 감속기
진단 프레임워크
서수 패턴 분석
모션 분리
분포기반 고장감지

학번: 2019-22571